DOE/NASA/0067-79-3
NASA CR-165317

TECHNOLOGY DEVELOPMENT FOR PHOSPHORIC ACID FUEL CELL POWERPLANT (PHASE II): 6TH QUARTERLY REPORT

LARRY CHRISTNER
ENERGY RESEARCH CORPORATION

MARCH 1980

PREPARED FOR
NATIONAL AERONAUTICS AND SPACE ADMINISTRATION
LEWIS RESEARCH CENTER
UNDER CONTRACT DEN3-67

FOR
U.S. DEPARTMENT OF ENERGY
ENERGY TECHNOLOGY
DIVISION OF FOSSIL FUEL UTILIZATION

DOE/NASA/0067-79-3
NASA CR-165317

TECHNOLOGY DEVELOPMENT FOR PHOSPHORIC ACID FUEL CELL POWERPLANT (PHASE II): 6TH QUARTERLY REPORT

LARRY CHRISTNER
ENERGY RESEARCH CORPORATION
3 GREAT PASTURE ROAD
DANBURY, CONNECTICUT 06810

MARCH 1980

PREPARED FOR
NATIONAL AERONAUTICS AND SPACE ADMINISTRATION
LEWIS RESEARCH CENTER
CLEVELAND, OHIO 44135
UNDER CONTRACT DEN3-67

FOR
U.S. DEPARTMENT OF ENERGY
ENERGY TECHNOLOGY
DIVISION OF FOSSIL FUEL UTILIZATION
WASHINGTON, D.C. 20545
UNDER INTERAGENCY AGREEMENT DE-AI-03-79 ET11272

EXECUTIVE SUMMARY

Technology development continued for materials, cell components, and short and long stacks. Significant progress made during the quarter is summarized below.

Component Development

- The use of 1000 grit silicon carbide as-received, without cleaning, results in a more porous matrix. This more advantageous matrix can therefore be prepared in less time.
- A 25 cm^2 cell test using the uncleaned SiC matrix operated at 200 mA/cm^2 and 650 mV.
- A computer program has been developed for predicting the start-up and operating conditions which minimizes the change in acid volume. It can also determine the volume changes which occur when the operating conditions are changed.
- Several 25 cm^2 test cell plates have been carbonized at approximately 900°C. Test cells built with these plates have been operating during the quarter with excellent performance.
- A retort for heat treating 1200 cm^2 test cell plates has been built.

Material Evaluation

- The corrosion rates of graphite/resin composites were easily distinguishable only after 500 hours of immersion in hot phosphoric acid. Corrosion is very rapid at 0.9V, 190°C in 100% H_3PO_4 and probably occurs by a different mechanism than at 0.6 to 0.8V.
- There is a significant decrease in the corrosion rate within the first 124 hours at 0.9V in 182°C, 100% H_3PO_4.
- Carbonization at 900°C lowers the corrosion rate by as much as a factor of 10.
- A graphic method has been successfully applied to the determination of contact resistivities of bipolar plate materials and electrode backing papers.
- Estimates of stack resistance from material resistivity measurements can account for the major contributors. Contact resistance between the backing paper and the bipolar plate is about 1/3 of the estimated resistance.

- An empirical correlation between applied stack compression and contact resistivity ($\rho_2 = \frac{C_1}{p} + C_2$) was obtained.

Endurance Testing

- Although Kynol matrix stacks have shown stable operation for over 7,000 hours they appear to be less reliable than SiC and Mat-1 matrices.
- SiC and Mat-1 matrix stacks have operated for 4,000 hours with very little change in the average cell voltage. Small changes are occuring in the end cells of the three cell stacks. This may be due to temperature gradients in these end cells.

Short Stack Testing

- Two 1200 cm^2 cell stacks containing 5 cells/ stack have run for over 1,000 continuous hours. These stacks were built with new 1200 cm^2 cell bipolar plates containing a wicking channel and components prefilled with acid.

Long Stack Testing

- The second 23 cell stack was operated for 40 hours net running time with daily on/off cycling. A crossleak developed after the 7th cycle. The next 23 cell stack will incorporate bipolar plates with wicking channels and the Mat-1 matrix.
- The electrically heated reformer has demonstrated the capability to reform methane at a space velocity of 1200 hr^{-1} and provide sufficient hydrogen to test a 23 cell stack.

TABLE OF CONTENTS

TABLE OF CONTENTS (cont.)

LIST OF FIGURES

LIST OF FIGURES
(Concluded)

ENERGY RESEARCH CORPORATION

LIST OF TABLES

TASK I. COMPONENT DEVELOPMENT

1.1 MATRIX DEVELOPMENT

Prior to being used in a matrix, all SiC was routinely "cleaned". This cleaning consisted of vigorously mixing (in a ball mill or ultrasonically) the SiC in deionized water and allowing it to settle. A small fraction of the material floats to the surface as a black sheen and is skimmed off. An additional small fraction of the material is brown and remains suspended in the water. This material is poured off with the water and the rest of the SiC is dried and used for matrices. It has long been suspected that this brown and black material is simply impure SiC (i.e., an excess of unreacted carbon could cause the black color, etc.) as opposed to the "pure" green SiC desired because of its greater resistance to phosphoric acid. Recent chemical analyses performed for ERC have shown no detectable difference between cleaned and uncleaned SiC. If the difference in chemical content is, in fact, insignificant, then the time consuming cleaning step could be eliminated from the matrix production process.

A 25 cm^2 test cell was made with a matrix containing uncleaned SiC. Cell 104 (Table I.1) started up well and is producing 650 mV at 200 mA/cm^2 on an IR corrected basis. The O_2 gains are small and there is as yet no sign of cell poisoning due to the leaching of contaminants from the matrix. Cells 105 and 106 (Table I.2) which contain selectively wet-proofed anode backings, were also built with the same cathode and matrix as Cell 104 and are performing at acceptable levels. They will be discussed further in Section 1.3.1. It should be noted, however, that three matrices cast with uncleaned SiC have all been 50% thicker than matrices cast with clean SiC (0.023 vs 0.015 cm) and have ranged from 59 to 63% in porosity, which is approximately 20% more porous than the average matrix (51% porous) made with clean SiC. All other casting parameters have remained constant. The increase

ENERGY RESEARCH CORPORATION

TABLE I.1

CELL TESTING SUMMARY

CELL NO.	1409	1426	104
TEST OBJECTIVE	Ball Milled SiC Matrix	Prewashed Backings	Uncleaned SiC Matrix
CELL CHARACTERISTICS			
ANODE			
Type	Rolled	Sheet Mold	Sheet Mold
TFE, %	40	40	40
Loading, mg Pt/cm^2	0.49	0.29	0.32
CATHODE			
Type	Rolled	Sheet Mold	Rolled
TFE, %	40	40	40
Loading, mg Pt/cm^2	0.53	0.70	0.62
MATRIX	SiC	Kynol	SiC
TFE, %	4	--	4
Porosity, %	--	--	62
Thickness, cm	0.013	0.040	0.023
Sintering	15 min @ 330°C	--	15 min @ 330°C
ANODE BACKING % FEP	38	33	34
CATHODE BACKING % FEP	38	31	39
PEAK PERFORMANCE, mV IR Free			
AIR - 100 mA/cm^2	710	666	700
200 mA/cm^2	660	613	650
O_2 - 100 mA/cm^2	780	726	770
200 mA/cm^2	730	690	720
O_2 - AIR - 100 mA/cm^2	70	60	70
200 mA/cm^2	70	77	70
PRESENT PERFORMANCE			
AIR - 200 mA/cm^2	*	*	650
CELL LIFE, hours	2424	2192	216

* Test Terminated

TABLE I.2

TESTING SUMMARY OF AICM CELLS

CELL NO.	1345	1378	100	101	102	103	105	106
TEST OBJECTIVE	Large Sheet Mold Electrodes & AICM Control	AICM	AICM	AICM	AICM	AICM	AICM	AICM
CELL CHARACTERISTICS								
ANODE								
Type	Sheet Mold	Rolled	Rolled	Rolled	Rolled	Rolled	Rolled	Rolled
TFE, %	40	40	40	40	40	40	40	40
Loading, mg Pt/cm^2	0.45	0.3	0.35	0.33	0.32	0.30	0.33	0.33
CATHODE								
Type	Sheet Mold	Rolled	Rolled	Rolled	Rolled	Rolled	Rolled	Rolled
TFE, %	40	40	40	40	40	40	40	40
Loading, mg Pt/cm^2	0.50	0.5	0.56	0.56	0.50	0.65	0.62	0.62
MATRIX	Kynol	SiC	SiC	SiC	SiC	SiC	SiC	SiC
TFE, %	--	4	4	4	4	4	4	4
Porosity, %	--	--	--	--	--	--	62	62
Thickness, cm	0.048	0.015	0.015	0.015	0.015	0.020	0.023	0.023
Sintering	--	15 min @ 330°C	15 min @ 330°C	15 min @ 330°C	15 min @ 330°C	15 min @ 330°C	15 min @ 330°C	15 min @ 330°C
ANODE BACKING % FEP	35	11.6	27	36	24	25	35	35
CATHODE BACKING % FEP	34	39	36	36	40	37	39	39
PEAK PERFORMANCE, mV IR-Free								
Air - 100 mA/cm^2	733	705	671	653	663	665	686	677
200 mA/cm^2	685	650	648	607	607	600	635	624
O_2 - 100 mA/cm^2	793	770	733	716	726	726	746	742
200 mA/cm^2	775	740	690	671	689	675	703	700
O_2 GAIN - 100 mA/cm^2	60	65	62	63	63	61	60	65
200 mA/cm^2	90	90	42	78	82	75	68	76
PRESENT PERFORMANCE								
AIR - 200 mA/cm^2	685	*	612	*	*	596	635	624
CELL LIFE, hours	6456	3720	1272	1176	1008	744	96	48

* Test Terminated

in porosity of uncleaned SiC is an unexpected dividend. Since the particles removed in cleaning are finer than the ones that remain, it might have been expected that they would fill the spaces between the larger particles creating a less porous matrix; but apparently they create a more structured, less densely packed matrix. This work will be continued and cells containing uncleaned SiC matrices will be closely monitored.

The evaluation of ball milled SiC slurries begun during the last quarter was continued this quarter and has been successfully concluded. The method produces uniform slurries without excessive degradation of the shear sensitive inking vehicle and has been used to produce numerous, good quality 1200 cm^2 and smaller matrices. Cell 1409 (Table I.1) which was designed specifically to test the matrix was still at peak performance when terminated after more than 2400 hours.

1.2 COMPONENT SCALE-UP

The scale-up of 1200 cm^2 sheet mold and rolled electrodes and SiC matrices is essentially complete. There are no major difficulties in the processes themselves, although improvements affecting the rate of production and the performance of the components will, of course, continue.

Stack 415, containing sheet mold electrodes, was started up during this quarter. It reached a peak terminal performance of 0.59V/cell and is presently averaging 0.57V/cell after almost 1100 hours.

1.3 DEFINITION AND CONTROL OF ELECTROLYTE VOLUME CHANGES

1.3.1 Acid Inventory Control Members

A number of new cells with selectively wetproofed anode backings as AICMs (Cells 100,101, 102, 103, 105 and 106) were tested during this quarter (Table I.2). The electrodes in Cells 100, 102 and 105 were wet with acid during assembly, while the anodes in Cells 101, 103 and 106 were partially

float filled prior to assembly. Since the AICMs are expected to absorb changes in acid volume, the prefilling of anodes in some of the cells may be considered an attempt to accelerate what will happen eventually in the other cells. The extent to which filling the backings with acid interferes with the flow of hydrogen to the anodes has a great deal to do with cell performance. The average peak performance of the prefilled cells is only 610 mV, while the average of cells not prefilled is 630 mV, all at 200 mA/cm^2, IR corrected. Analysis of cell polarization curves indicates that, to a large extent, cell performance is indicative of backing flooding rather than catalyst flooding. The oxygen gains remain fairly low, while the drop in performance is steep as the load increases. This is the kind of performance that occurs when part of the catalyst area is effectively lost to use, rather than the kind of diffusion polarization that occurs when the catalyst is flooded.

Table I.3 relates cell performance to the cross-sectional area of the anode backing wetproofed and to the amount of acid picked up during prefilling. The percent of FEP in the backings is higher than might be expected because the FEP used for selective wetproofing was of a much higher concentration than is commonly used in the standard wetproofing operation. This was necessary due to the greater tendency of dilute FEP emulsions to spread out. The approximate percent of area covered by the FEP (listed in the next column) indicates that in these wetproofed areas, there is a much greater concentration of FEP than normal. The effect of this on the uniformity of current flow through the backings has not yet been determined. The next column lists the amount of acid that was picked up by the anode during prefill. All of the anode loadings were approximately 0.3 mg Pt/cm^2. By way of comparison, a typical electrode of that loading would pick up 0.11 cc of acid, presumably all in the catalyst layer. The next column shows the amount of acid that would be stored in an equivalent anode scaled to 1200 cm^2 size. Efforts will continue to define the amount of acid storage needed

TABLE I.3

TESTING SUMMARY OF 25 cm^2 AICM CELLS

CELL	PEAK PERFORMANCE, mV @ 200 mA/cm^2 IR-free	ANODE BACKING, Wt% FEP	FEP COVERED AREA, Approx. %	ACID PICKED UP IN PRE-FILL, cc	ACID IN EQUIV. 1200 cm^2 ANODE,cc	PEAK O_2 GAIN,mV @ 200mA/cm^2
100	648	27	25	None	0	42
101	607	36	28	0.283	13.4	78
102	607	24	46	None	0	82
103	600	25	40	0.338	16.0	75
105	735	35	40	None	0	68
106	624	35	40	0.434	20.5	76

and to optimize the degree and pattern of wetproofing.

As stated previously*, Cell 1345 (Table I.2) was used as a control in an experiment designed to determine the effect of acid deprivation on cells with AICMs. It has since been used to study the ability of a cell to recover from extended electrolyte starvation. The cell was deprived of acid for a period of six weeks, during which time its terminal OCV and performance at load dropped while its internal resistance (IR) increased. The decrease in performance was almost entirely due to the increased IR. When acid was added, the IR-free performance shortly before and after acid addition was identical: 615 mV at 200 mA/cm^2. The decrease in IR-free performance caused by six weeks without acid addition was approximately 25 mV. In the seven weeks since regular acid addition was resumed, cell terminal voltage has remained relatively stable while IR has increased again to the point where, after almost 6500 hours, Cell 1345 has reached a new IR-free peak of 685 mV at 200 mA/cm^2.

Cell 1378 (Table I.2) was a very successful 25 cm^2 AICM test cell, as previously reported. It was terminated after more than 3700 hours due to an increasingly severe short.

Stack 417, a 1200 cm^2 stack containing anode backings with only 20% FEP, was started up during this quarter and peaked at an average of 560 mV/cell at 100 mA/cm^2. However after 800 hours, stack performance has dropped to an average of 500 mV/cell, apparently due to flooding. Stack 417 is reported in greater detail in Task IV.

1.3.2 Procedures for Wicking and Starting the Stack

Optimal paths were prepared for stack wicking and starting to prevent acid drippage and weeping from the cells. Figure I.1 shows the steps for computing optimal cell conditions from wicking to final operation. In the calculations, final stack operating conditions were assumed to be 175°C and 100

---

* ERC Technical Progress Report DEN3-67, No. 5, Oct - Dec. 1979

ENERGY RESEARCH CORPORATION

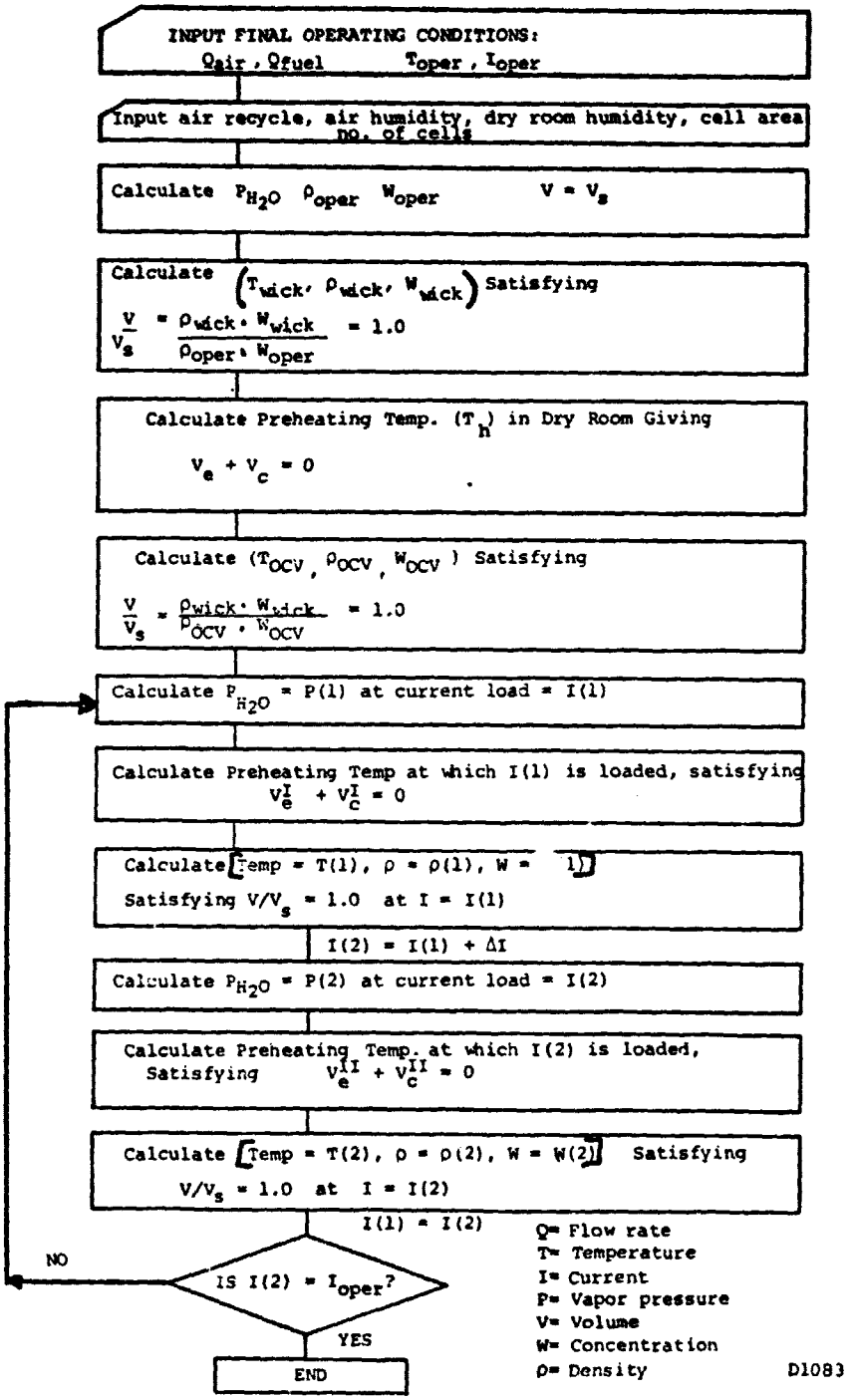

FIGURE I.1

FLOW CHART FOR CALCULATING STACK WICKING AND STARTING CONDITIONS

mA/cm^2. From the information of flow rates, humidities of air and fuel, and current load, the partial water vapor pressures on the cathode and anode are estimated from overall mass balance equations. Acid density and concentration are then calculated from the correlated equations, using the estimated water vapor pressure on the cell. Based on the saturated cell condition at final stack operating conditions, an optimal wicking condition can be determined from the following equation:

$$\frac{\text{Vol. of acid in cell at wicking}}{\text{Vol. of acid in cell during operation}} = \frac{\rho_{wick} \cdot W_{wick}}{\rho_{oper} \cdot W_{oper}} = 1.0$$

Where,

ρ_{wick} and ρ_{oper} = densities

W_{wick} and W_{oper} = concentrations

} at wicking and operating stages, respectively.

Using this equation, a wicking temperature can be calculated by an iterative method (See also appendix A and B).

After wicking, the stack is preheated in the dry room prior to OCV testing under higher humidity conditions. Figure I.2 illustrates the point (T_h) to which the stack should be preheated in the dry room. As shown, the volume of acid in the cell will expand when the stack is placed under higher humidity, and gradually shrink as the stack is heated. The behavior of volume change with temperature will depend on the rate of moisture absorption, i.e., curve r_1 represents the case of an infinitely fast absorption rate. When the rate is very slow, the volume expansion curve will become almost flat to approach the T-axis. The preheating temperature is determined, based on the extreme condition of the moisture absorption rate, to insure safety when the stack is standing for a prolonged period outside the dry room. At point T_h, volume contraction and expansion become identical inside and outside

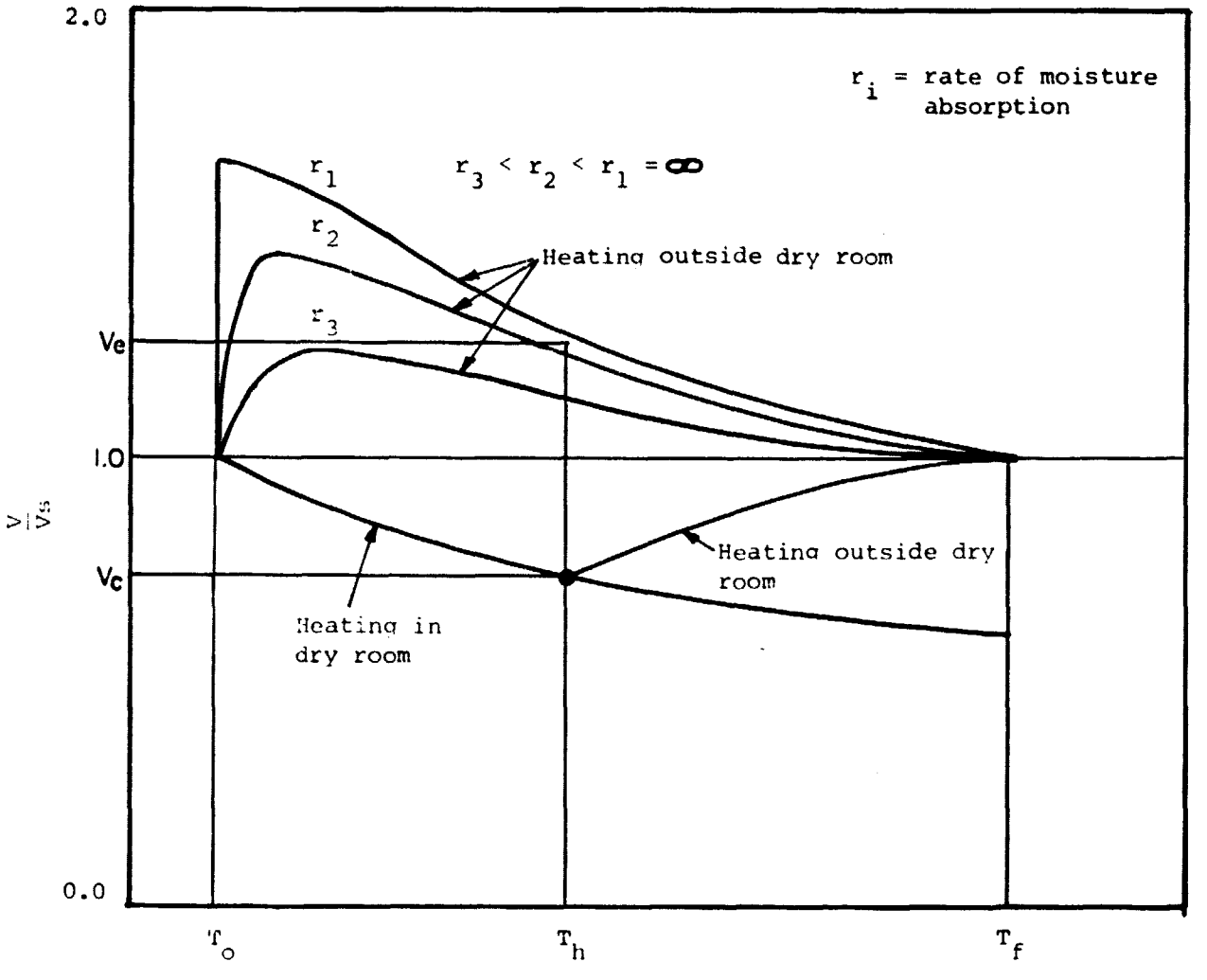

FIGURE I.2 ACID VOLUME BEHAVIOR DURING HEATING AT TWO DIFFERENT HUMIDITIES

D1153

the dry room, respectively. The stack is then moved out of the dry room to a test stand to continue heating until the acid volume returns to the saturation point, before OCV testing. The temperature for OCV measurement is similarly determined, as described above for wicking temperature determination. Then the stack is again preheated to reduce the acid volume in the cell before loading current on the stack. Figures I.3 through I.8 illustrate calculated paths to be followed from wicking to a final operating condition.

In Figure I.3 a three dimensional path was drawn for an air stoch* of 3.0, dry room humidity of 2.5 mm Hg, and a testing lab humidity of 12 mm Hg. Under the given conditions, the optimal wicking temperature becomes 75°C and the acid concentration is 97.6%. After wicking, the stack is preheated to 99.5°C (path a-b), before taking it out of the dry room to the 12 mm Hg humidity condition and heating it to 120°C (path b-c) before OCV testing. After OCV measurements, the stack is kept at 123°C (path c-d) before the 20 mA/cm^2 current loading. After the stack is put on load, the temperature is raised to 126°C (path d-e). When the starting current loads are 40, 60, 80 and 100 mA/cm^2, the preheating temperatures become 130, 142, 152 and 162°C, as shown in the figure.

The steps can be described more clearly by redrawing the path on a P_{H_2O}-temperature plane (Figure I.4). In Figures I.5 and I.6, two different paths for dry room humidities of 1.5 and 2.5 mm Hg† are being compared on a volume - temperature plane for air stoichs of 2 and 3. As shown, the dry room humidity changes the wicking and preheating temperatures, keeping the rest of the steps unchanged. For an air stoich of 2, humidities of 1.5 and 2.5 mm Hg give wicking temperatures of 59 and 71°C, respectively. Figure I.7 shows the path deviation when the testing lab humidity increases from 12 to 16 mm Hg.

---

* Through the cathode channels.

† Equivalent to 6 and 10% relative humidity at 25°C.

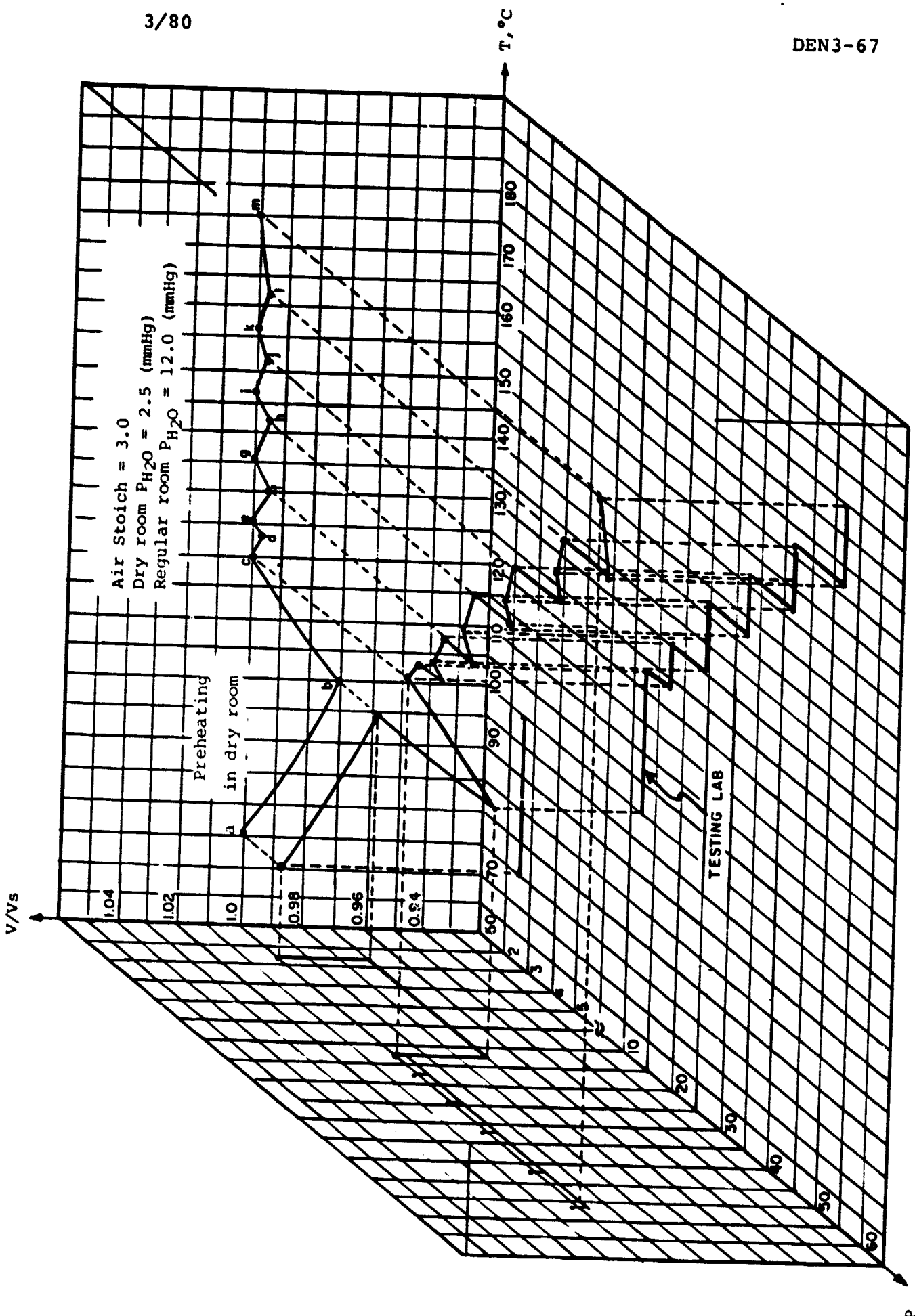

D1163

FIGURE I.3 PATH TO BE FOLLOWED FROM WICKING TO OPERATING CONDITION

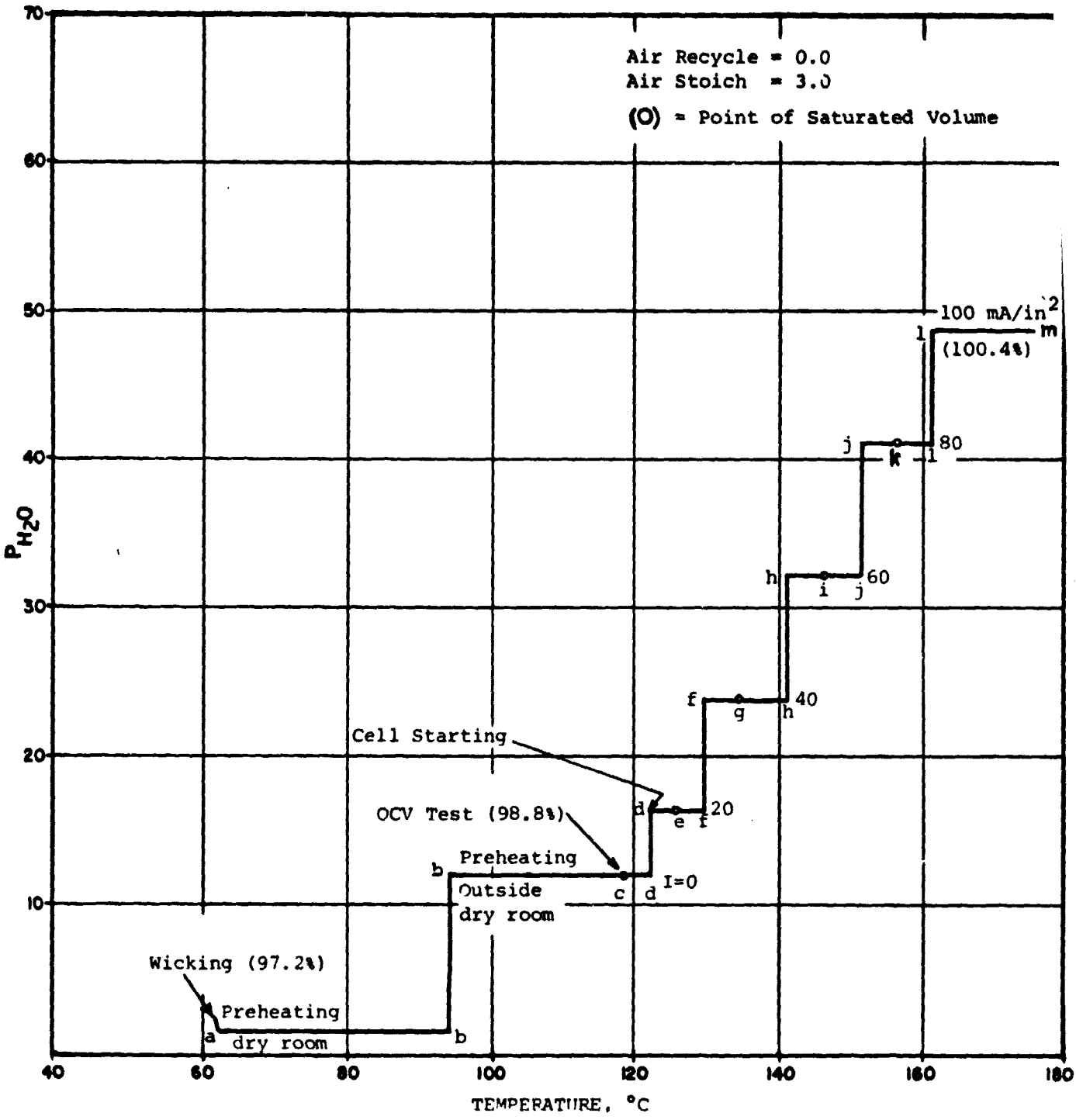

FIGURE I.4 STEPS TO BE FOLLOWED ON P_{H_2O} - TEMPERATURE PLANE

D1162

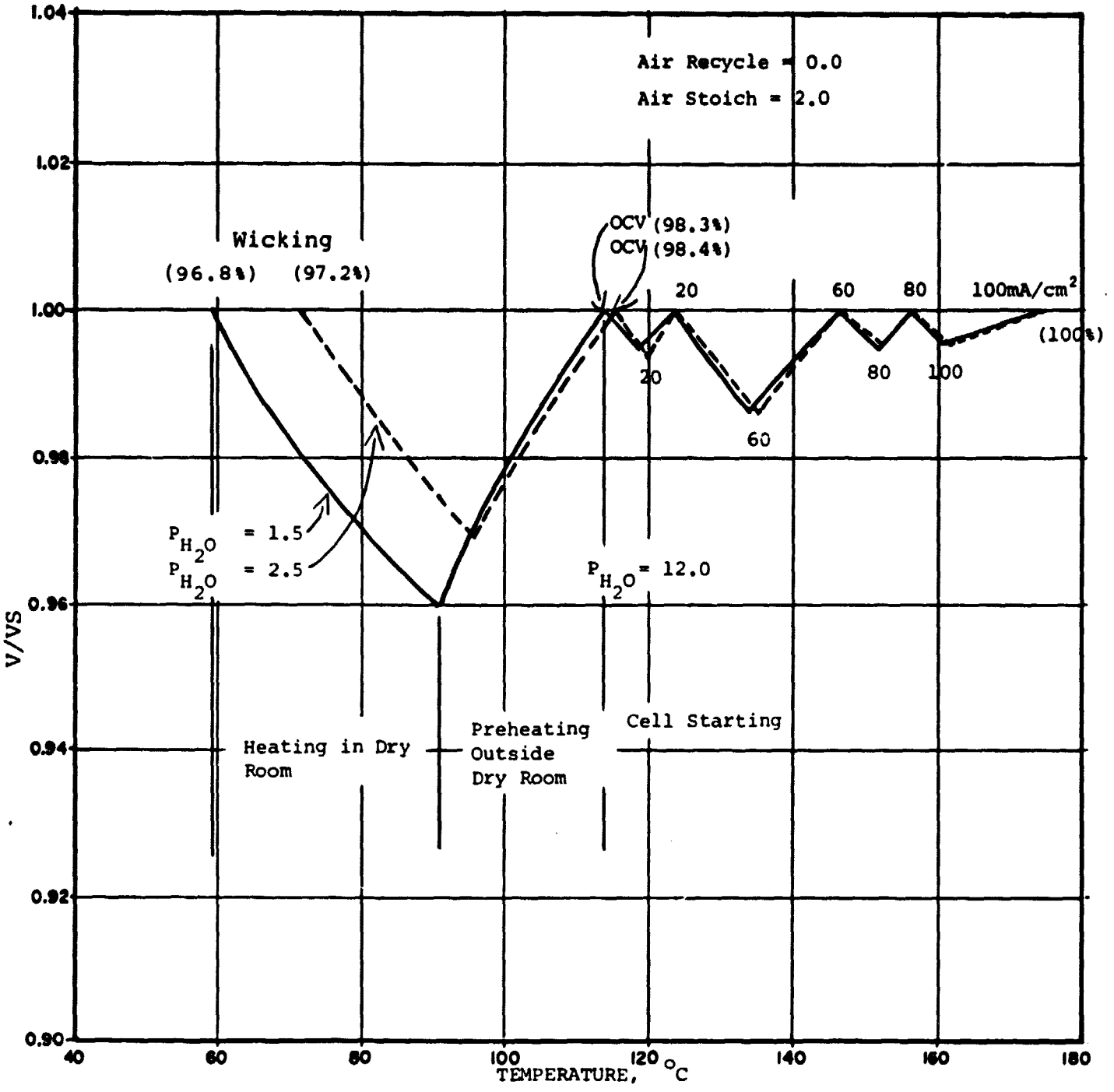

FIGURE I.5 COMPARISON OF PATHS ON A VOLUME - TEMPERATURE PLANE FOR TWO DIFFERENT DRY ROOM HUMIDITIES FOR AIR STOICH = 2.0

D1158

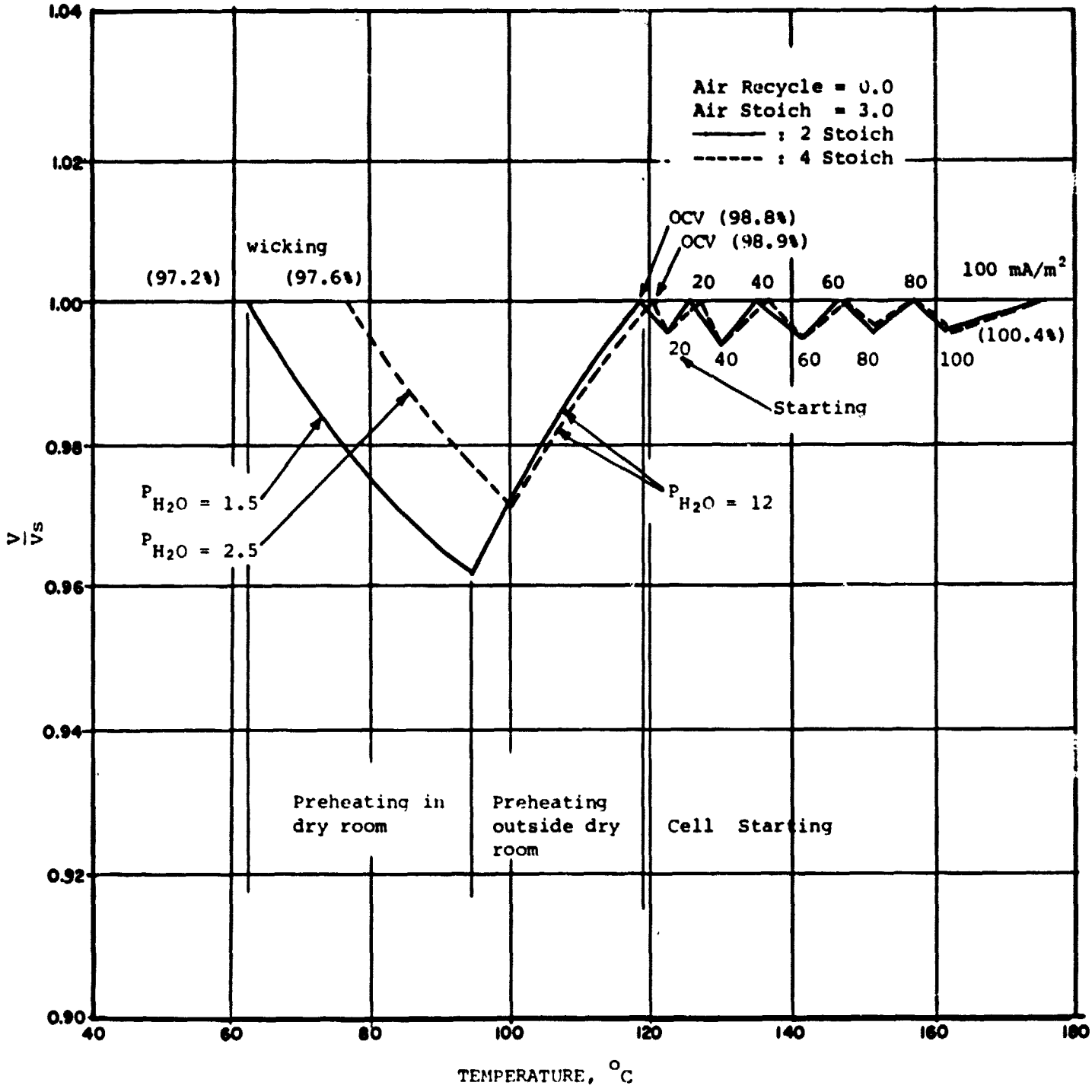

FIGURE I.6 COMPARISON OF PATHS ON VOLUME-TEMPERATURE PLANE FOR TWO DIFFERENT DRY ROOM HUMIDITIES FOR AIR STOICH = 3.0

D1159

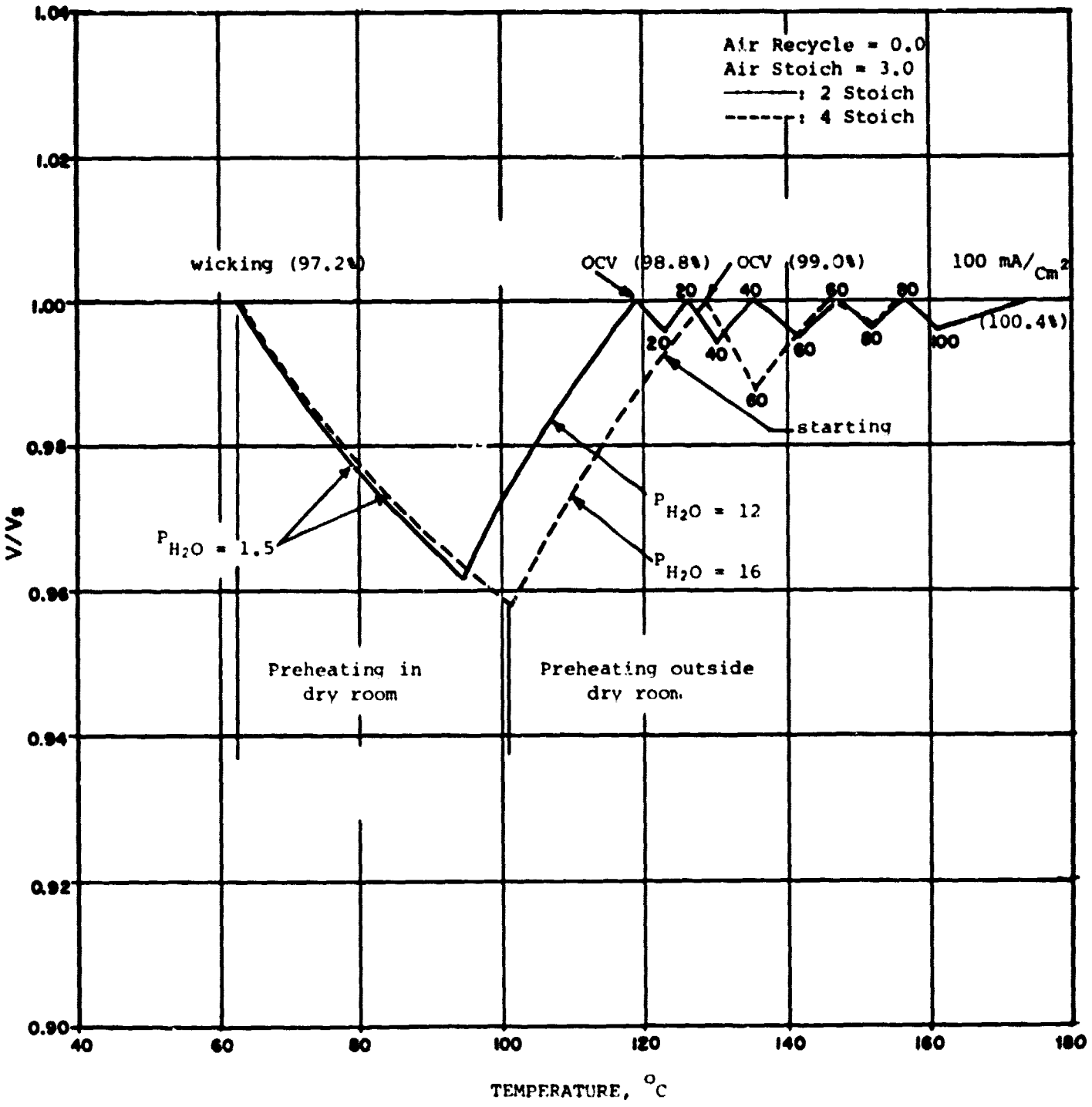

FIGURE I.7 COMPARISON OF PATH DEVIATION WHEN ROOM HUMIDITY IS INCREASED FROM 12 TO 16 mm Hg

D1160

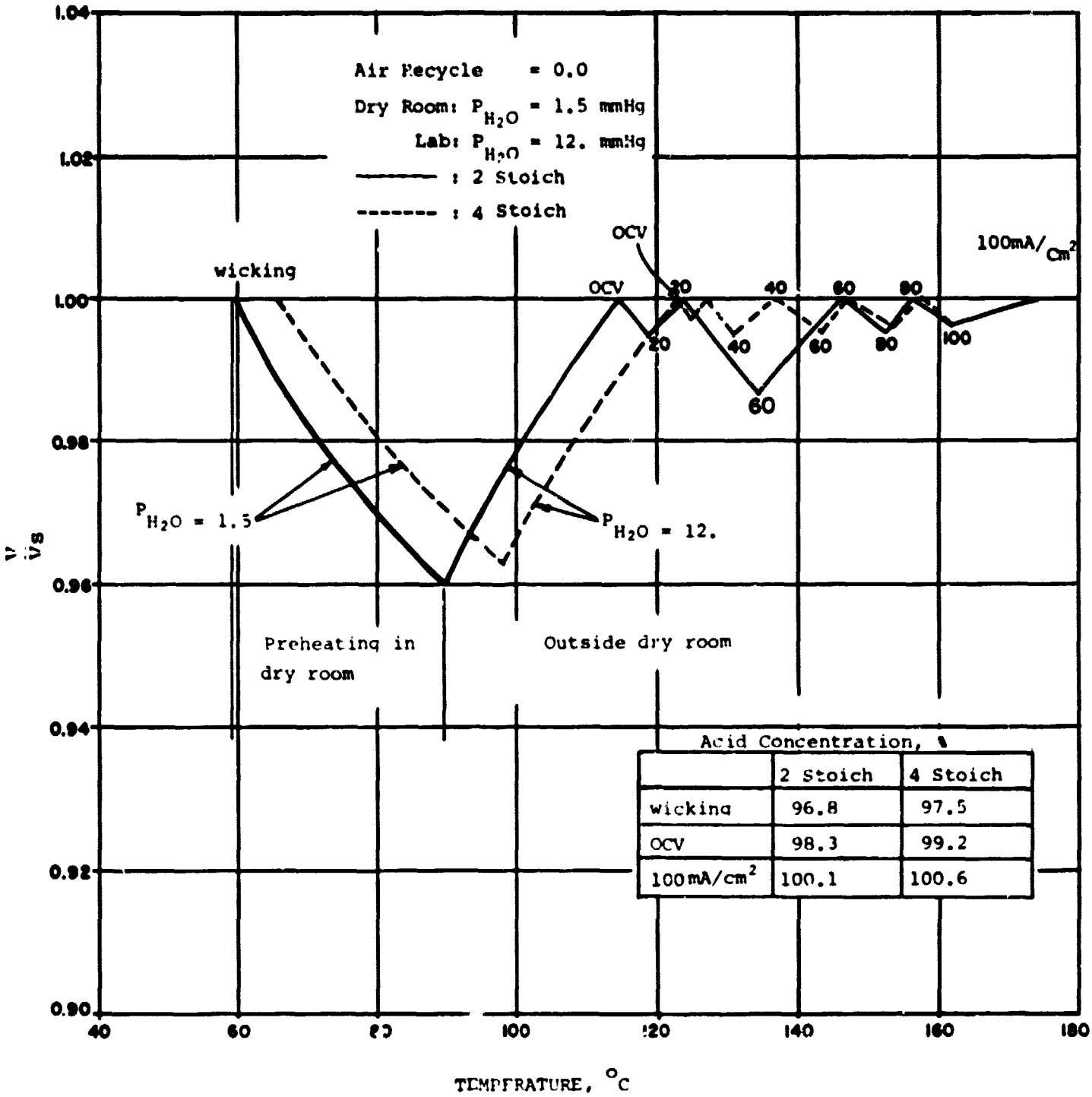

Acid Concentration, %

	2 Stoich	4 Stoich
wicking	96.8	97.5
OCV	98.3	99.2
100 mA/cm²	100.1	100.6

FIGURE I.8 COMPARISON OF PATH DEVIATION WHEN AIR FLOW IS INCREASED FROM 2 TO 4 STOICH

D1161

In this situation, the temperature for OCV testing changes from 119 to 128°C. Figure I.8 compares two different paths for two different air flow stoichs of 2 and 4. The higher flow rate gives a higher wicking temperature since higher flow increases the acid concentration in the cell.

Table I.4 summarizes a comparison of stack conditions from wicking to starting for 2 and 4 air stoichs, and for zero and 40% recycling of air. According to the table, wicking temperature varies from 59 to 77°C, preheating temperature in the dry room varies from 91 to 108°C, and temperature for OCV testing varies from 114 to 130°C. Based on this information given in the table, a set of stack parameters was chosen to allow tolerance of the varying environment within reasonably small volume changes. Table I.5 shows the recommended parameters to be applied from stack wicking to starting. Maximum volume expansion encountered for the given set of parameters was estimated to be 2.5%.

In the next quarter, optimal flow and temperature conditions will be determined to keep the acid volume unchanged in the cell throughout the starting period.

TABLE I.5 RECOMMENDED SET OF PARAMETERS

WICKING	PREHEATING IN DRY ROOM	OCV TESTING	STARTING
T = 70 W = 97	T = 110	T = 120 W = 99	T = 150 I = 60

Units: T (°C); W (%); I (mA/cm^2)

TABLE I.4

COMPARISION OF STACK CONDITIONS* FROM WICKING TO STARTING

AIR STOICH	ZERO RECYCLE										40% RECYCLE									
	WICK			PREHEAT		OCV TEST			START		WICK			PREHEAT		OCV TEST			START	
	P_{H_2O}	T	W	P_{H_2O}	T	P_{H_2O}	T	W	I	T	P_{H_2O}	T	W	P_{H_2O}	T	P_{H_2O}	T	W	I	T
2	1.5	59	96.8	1.5	91	12	114	98.3	60	135	1.5	57	96.5	1.5	88	12	112	98	60	134
				1.5	97	16	124	98.6	60	132				1.5	94	16	120	98.3	60	134
	2.5	71	97.2	2.5	96	12	115	98.4	60	135	2.5	69	96.8	2.5	92	12	111	98	60	134
				2.5	101	16	125	98.7	60	133				2.5	98	16	120	98.3	60	131
4	1.5	65	97.5	1.5	98	12	123	99.2	60	143	1.5	63	97.2	1.5	95	12	119	98.8	60	135
				1.5	104	16	130	99.6	60	143				1.5	101	16	128	99	60	135
	2.5	77	97.8	2.5	102	12	122	99	60	142	2.5	75	97.6	2.5	100	12	120	98.9	60	142
				2.5	108	16	130	99.6	60	142				2.5	105	16	130	99.2	60	135

Units: P_{H_2O} (mm Hg); T(°C); W(%); I(mA/cm^2)

* Based on final operating conditions: 100 mA/cm^2 and 175°C .

1.4 BACKING PAPER TECHNOLOGY

The previously reported variabliity of wetproofing in 1200 cm^2 backings is the result of a technique which involves dipping the backings in a dilute FEP suspension and then draining off the surplus liquid. During draining the backings are held by one end or corner and the FEP flows out of the top and concentrates at the bottom. Alternate draining techniques are being tried including rotating the backings during draining and lifting them out of the FEP on a screen. However the fragility of the backings and the awkwardness of handling them presents many difficulties. Attempts to solve these problems, possibly by other methods of FEP application, will continue.

Cell 1426 (Table I.1), which contains prewashed backings, was reported previously. Its performance was somewhat low, but very stable and it was terminated after almost 2200 hours. Analysis of the cell data does not indicate that the backing was responsible for the low performance.

1.5 BIPOLAR PLATE TECHNOLOGY

1.5.1 Molding

Molding trials with Varcum 24-655 resin from Reichhold Chemicals, Inc. were completed and molding trials with Varcum 29-703 resin were initiated. Production rates with the Varcum 24-655 resin were comparable to those of the current bipolar plates with Colloid 8440 resin from Colloid Chemical, Inc. The Varcum 24-655 resin is a one-stage phenolic resin and has a shelf life of 60 days at 16°C, while Varcum 29-703 and Colloid 8440 are two-stage resins. "Compounds formulated with two-stage resins have a greater molding latitude, better dimensional stability, and better long-term storage capabilities than with single-stage resins"*. Varcum 24-655 resin compounds were superior to Colloid 8440 resin compounds in corrosion resistance. The corrosion studies with H_3PO_4 showed Varcum 29-703 having comparable if not better corrosion resistance than Varcum 24-655.

* "Phenolic", Modern Plastics Encyclopedia, 1978-1979, 34.

Initial molding trials with Varcum 29-703 resin compounds indicated no potential problems in fabricating bipolar plates. The current resin prices for less than a truckload are:

Varcum 24-655:	$1.50/kg
Varcum 29-703:	$1.52/kg
Colloid 8440:	$1.74/kg

The standard bipolar plates in current use are 33 wt% Colloid 8440/67 wt% graphite. The graphite is composed of 27 wt% 850 and 73 wt% A-99 from Asbury Graphite Mills, Inc. As previously reported, the molding trials and physical property measurements showed no advantage in the usage of 850 graphite; therefore 850 graphite shall not be used in the fabrication of plates with Varcum 29-703 resin. The current graphite prices are:

Asbury Micro 850:	$4.85/kg
Asbury A-99	$ .86/kg

Current plans call for building 350 cm^2 and 1200 cm^2 stacks with bipolar plates of 32 wt% Varcum 29-703/ 68 wt% A-99, 25 wt% Varcum 29-703/ 75 wt% A-99, and carbonized 32 wt% Varcum 29-703/ 68 wt% A-99.

1.5.2 Carbonization

Carbonization runs 10 and 11 successfully carbonized subscale plates of 25 wt% Varcum 24-655/ 75 wt% A-99 by heating to a maximum temperature of 900°C in a nitrogen atmosphere. The plates were partially ribbed on one surface, flat on the other surface, and were 0.50 to 0.65 cm thick. The thickness of the plates required a 15 day heating cycle to avoid defects from outgassing. The cycle developed for standard bipolar plates (both sides ribbed and 40 to 46 cm thick) was five days.

The retort for carbonizing standard 1200 and 350 cm^2 bipolar plates is being fabricated and full scale plates will be carbonized during the next quarter.

ENERGY RESEARCH CORPORATION

TASK II MATERIAL EVALUATION

2.1 COMPONENT CORROSION RESISTANCE

2.1.1 Chemical Corrosion Measurements

A. Corrosion Characteristics of Resin-Graphite Composites:

Only the apparent corrosion rates (weight loss rate prior to correcting for acid absorption) of several composites were reported previously*. The true corrosion characteristics of some of these composites (evaluated from the initial 2000 hour corrosion measurement data of the controlled experiments) are discussed here.

Weight loss measurements of each sample type (in the time interval of 150 to 2000 hours) were observed to be linear with the time of acid immersion (Figure II.1). Contrary to expecta-

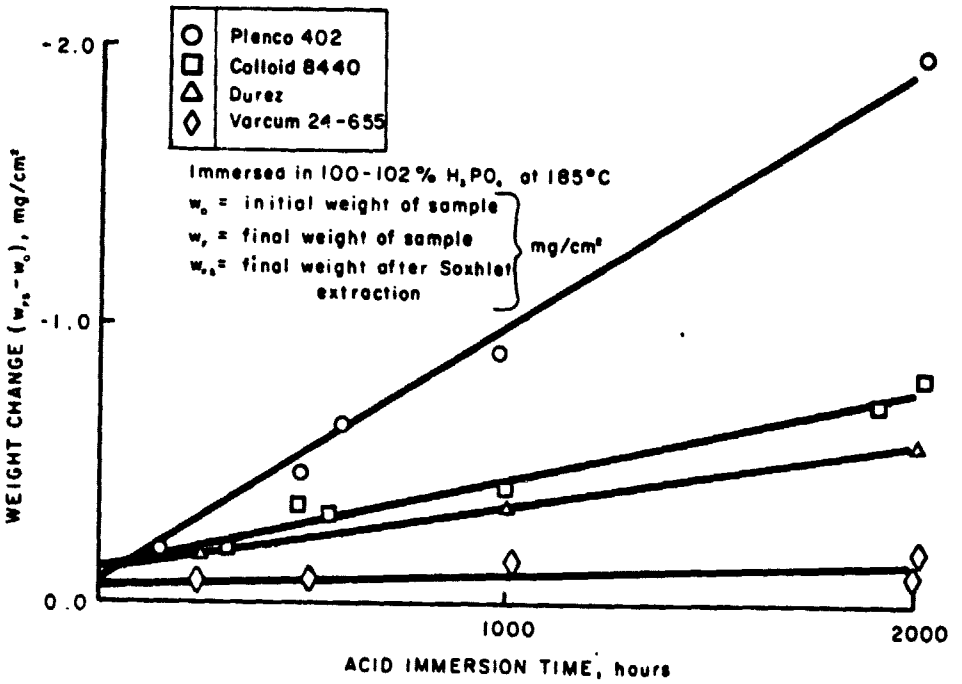

D1200

FIGURE II.1 TRUE CORROSION CHARACTERISTICS OF 22% RESIN/ 78% A-99 GRAPHITE COMPOSITES

* ERC Technical Progress Report DEN3-67, No. 4, July-Sept. 1979.

tions, these straight lines did not pass through the origin, raising the possibility that a higher rate of weight loss may be present during the early hours of acid immersion (<150 hours). Because of scatter in the acid absorption data, no attempt was made to define the acid absorption rate at this stage. The rate of weight loss for each of the composites, reported in Figure II.2, was calculated from the slope of the $(W_{fs}-W_o)$ vs time plot. The W_{fs} denotes the weight of the sample in g/cm^2 after aging in acid, extraction of acid with water and drying. W_o is the initial weight in g/cm^2 and t is the aging time in hours. Acid absorption of these samples at 2000 hours of aging, calculated from (W_f-W_{fs}), is also reported in Figure II.2. W_f is the weight of the aged sample after water washing and drying. The following observations can be made:

- Of the four samples compared, the Varcum 24-655 based composite has the lowest corrosion rate (-0.125 $\mu g/hr\text{-}cm^2$).
- Raising the resin content in the range of 22 to 32% seems to improve the corrosion rates of only those samples with high corrosion rates.
- In general, samples with higher acid absorption tend to have higher true corrosion rates.
- The acid absorption of each sample increases as the resin content decreases.

These findings are in accord with the SEM photographs of the corroded samples and also with our current notion of the corrosion mechanism, i.e., that corrosion mostly advances via crack propagation and that acid absorption takes place along these cracks.

In the future, corrosion measurement data up to 5000 hours will be used to update the true corrosion rates and to define the acid absorption characteristics for each of these composites. Experiments are also under way to investigate the possibility of the presence of a higher rate of weight loss during the initial hours (<150 hours) of acid immersion.

2.1.2 Electrochemical Corrosion Measurements

A. Potentiostatic Corrosion at 0.9V (RHE)

Several composite samples were studied under accelerated

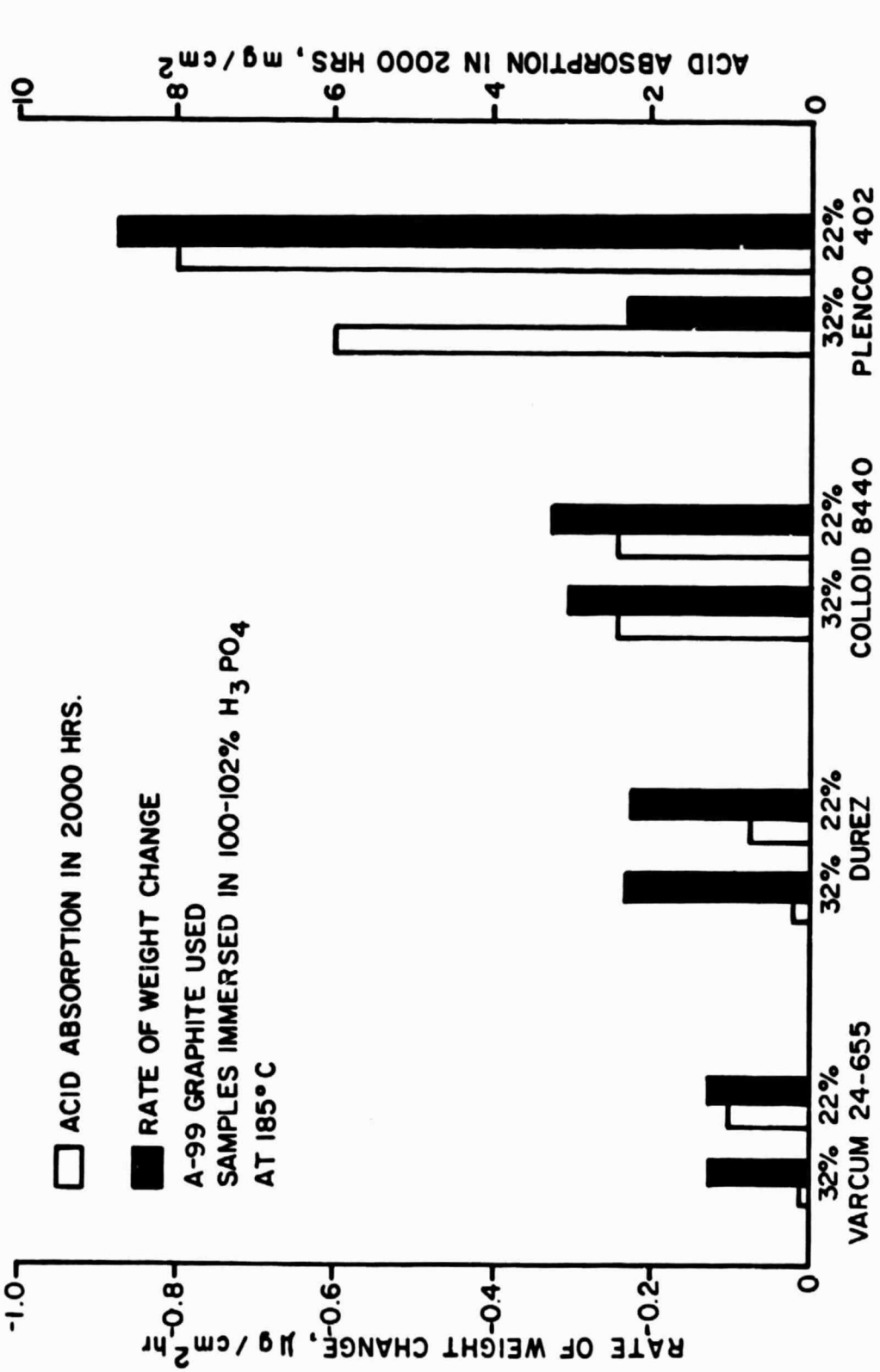

D1156

FIGURE II.2 ACID ABSORPTION IN 2000 HOURS AND THE TRUE RATE OF WEIGHT CHANGE OF SEVERAL COMPOSITES

potentiostatic corrosion conditions to evaluate the long-term relative corrosion characteristics.

Relative corrosion rates and the effects of resin content on corrosion rate and structural integrity of the sample were also studied. These samples were potentiostated at 0.9V (RHE) in 100 to 102% H_3PO_4 at 190.5°C (±0.5°C) in electrochemical polarization cells. The observed corrosion rates are plotted in Figure II.3 against time for four different samples: three contain 22% resin/78% A-99 graphite, and one sample contains 32% Varcum 24-655.

The current density is significantly high for all three bipolar 22% resin content composite plates. Probably the electrochemically active corrosion area is much larger than the exposed geometric area because the composite samples absorb acid. Furthermore, thin films of resin covering the carbon particles may also be polarized and reacted electrochemically in the process.

The corrosion rate decreased sharply for all 22% resin content samples after 140 to 200 hours of potentiostatic corrosion, depending on the sample type. It is speculated that beyond the point where the rate starts falling sharply, the structural integrity of the sample deteriorates rapidly.

The effect of resin content on the corrosion current is also reported in Figure II.3. The sample containing 32% resin has a lower corrosion rate. The corrosion current of the 22% Varcum sample is observed to be about 1.5 times higher than the 32% Varcum sample.

All the samples were post-tested; this consisted of visually checking for physical strength and other properties, and observing the samples under an ordinary microscope and a scanning electron microscope (SEM) for cracks, loss of surface integrity, blisters and etching pattern.

After termination of the experiment, the 22% Colloid and Plenco samples were found to be completely disintegrated. The 22% Varcum sample was just holding together but the mechanical

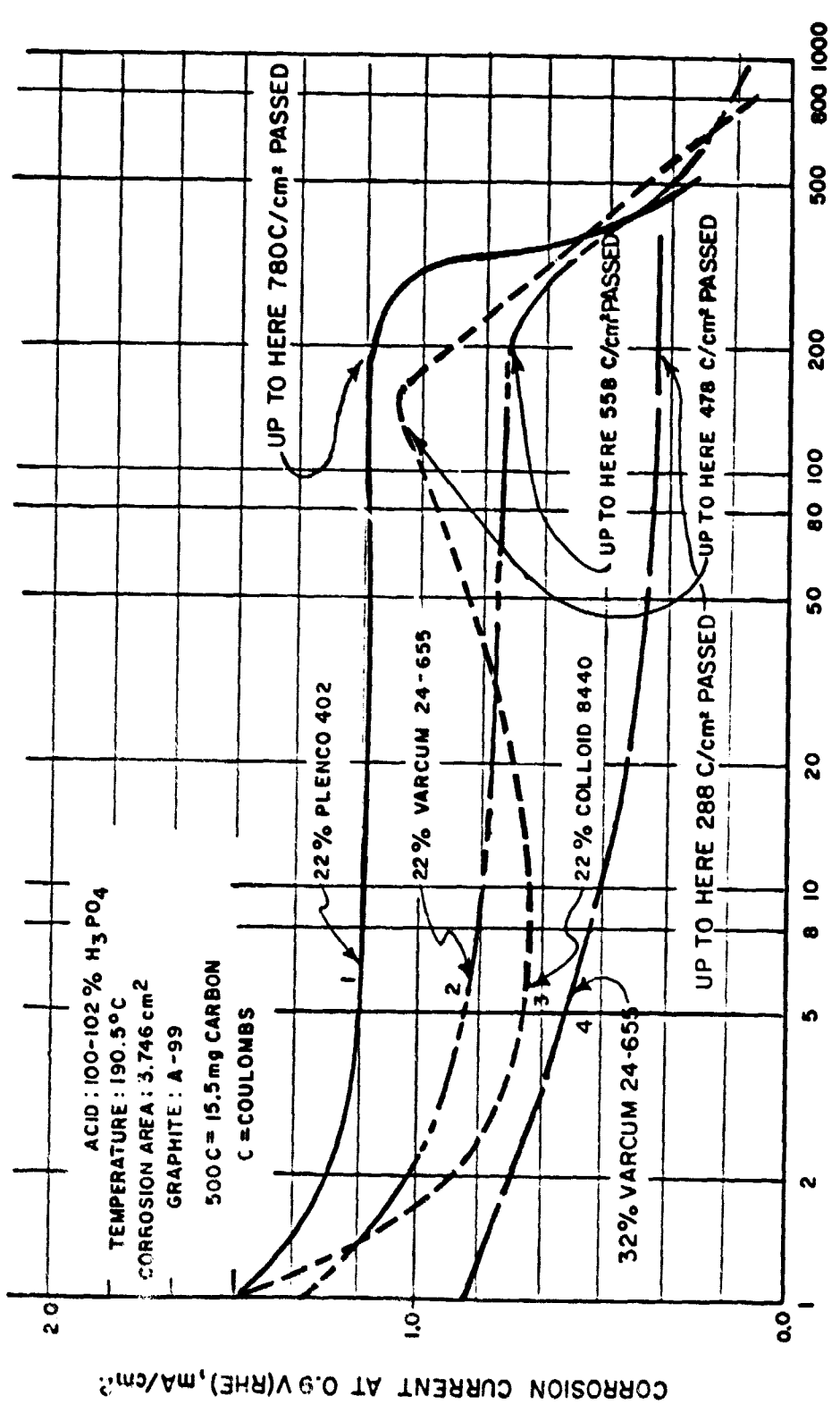

FIGURE II.3 CORROSION CURRENT OF COMPOSITES AT 0.9 VOLTS

properties seemed to have deteriorated greatly and tiny blisters (probably caused by electrochemical gas generation beneath the resin 'skin') were also observed on the surface of the sample. However there was no observable loss of physical strength in the cases of 32% Varcum 24-655 and 32% Varcum 29-703. Although SEM photographs did not reveal any sign of deterioration in structural integrity, tiny blisters were visible on the surface.

Photomicrographs of the electrochemically corroded and acid immersed samples are compared in Figure II.4. As the rate measurements revealed earlier (Figures II.2 and Figure II.3), surface photomicrographs also show that the electrochemical corrosion is much more severe. The absence of cracks on the surface of the electrochemically corroded sample indicates that the corrosion mechanisms may also be different. SEM photographs of the edges illustrate that in both the immersed and the corroded samples of 32% Varcum 24-655, corrosion is predominantly localized on the surface area.

The high rate of corrosion under electrochemical polarization conditions is probably related to: enhanced corrosion of carbon atoms at the binding sites; electrochemical oxidation of the resin present at the bond sites; and/or attack on the binding resin by the peroxide radical which is one of the plausible intermediates in the reaction pathway of graphite to CO_2.

Attempts are presently under way to compare the potentiostatic bipolar plate corrosion rates with pure A-99 graphite and glassy carbon corrosion rates and also to determine whether resins are oxidized during polarization. All long-term potentiostatic experiments to date have been performed at 0.9V but, in practice, the fuel cell operates in the potential range where the mechanism of corrosion is different. Therefore in a future experiment, long-term corrosion of a 22% Varcum 24-655 sample will be studied at 0.75V, where the corrosion mechanism differs from that which exists at 0.9V. In this way, it will be possible to determine whether the loss of sample structural integrity is

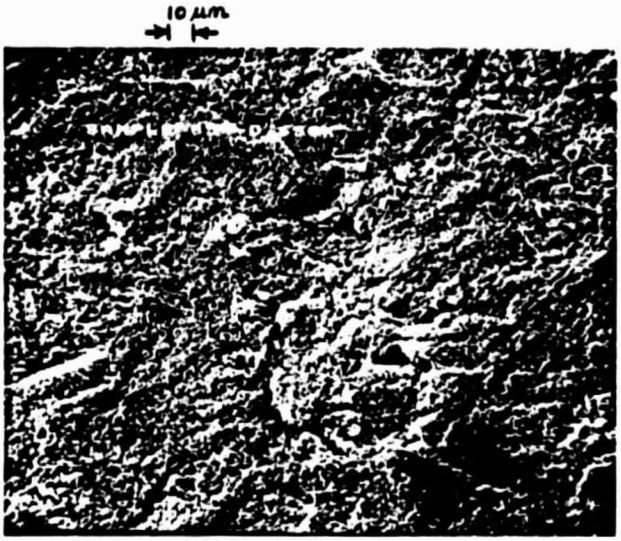

Unpolished surface (650X)

Polished Edge (500X) PO235

32% VARCUM 24-655 IMMERSED IN 100-102% H_3PO_4 AT 185°C FOR 1000 HOURS

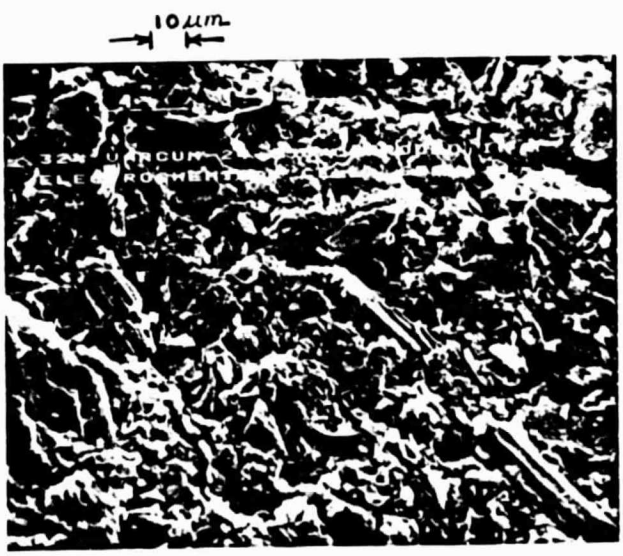

Unpolished surface (650X)

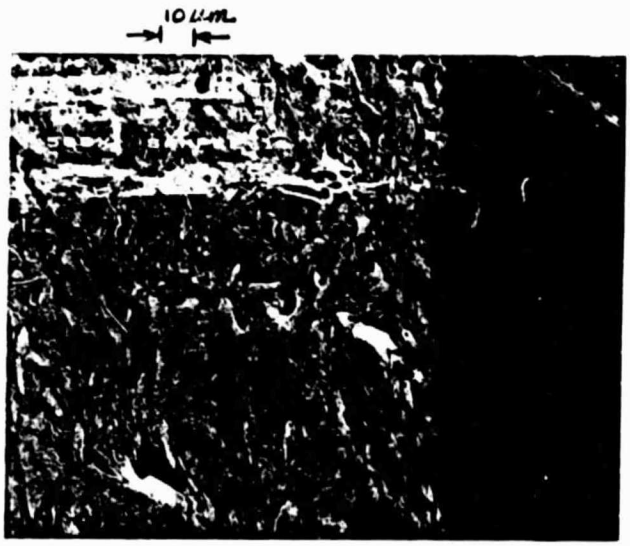

Polished Edge (500X) PO236

32% VARCUM 24-655 CORRODED IN 100-102% H_3PO_4 AT 0.9V AND 190°C FOR 360 HOURS

FIGURE II.4

COMPARISON OF ETCHED SURFACES OF ELECTROCHEMICALLY CORRODED AND ACID IMMERSED SAMPLES

potential dependent.

B. Polarization Study of Glassy Carbon

The kinetic parameters of the electrochemical corrosion reactions of bipolar plate materials were reported previously*. These results suggested high electrochemical corrosion currents for resin/graphite composite samples at fuel cell operating conditions. Attempts are under way to identify factors which contribute to the observed high current densities, and to determine the proper corrosion preventive measures. Thus a composite of cellulose and phenolic resin and a 100% Colloid 8440 sample were carbonized at about 900°C and subsequently studied in corrosion polarization experiments, as reported earlier for composite material*. Two different Tafel slopes, representative of two different reaction mechanisms, were also observed for this glassy carbon material in the potential range of 0.55 to 1.0V (RHE).

The corrosion currents for the carbonized composites were observed to be about an order of magnitude less than the non-carbonized ones. The kinetic parameters of the carbonized samples, summarized in Table II.1, were found to differ from the composite materials. Activation energies are much higher, hence the rate constants of glassy carbon electrochemical corrosion reactions would be significantly lower; this partly explains the low current densities observed. The true acid exposed areas of the carbonized and the graphite-resin composite samples, having the same geometric area, are probably different. Therefore in future experiments, the effect of this factor on the observed relative corrosion rates of these samples will be studied.

C. Corrosion Characteristics of Composites as the Reaction Proceeds

Using only the corrosion data of 'fresh' samples†, the

---

* DEN3-67, No. 5, Oct.-Dec. 1979

† After corroding at 0.9V (RHE) for 5 to 10 hours.

TABLE II.1 KINETIC PARAMETERS OF THE GLASSY CARBON CORROSION REACTION

CARBONIZED SAMPLE	TEMPERATURE, °C	Between 0.6 and 0.85V (RHE)				Between 0.875 and 1.05V (RHE)			
		Tafel Slope $b = \frac{PT}{\overleftarrow{\alpha}F} \times 2.303$ mV/decade	Transfer Coefficient $\overleftarrow{\alpha}$	Exchange Current Density i_o $(A/cm^2) \times 10^6$	Activation Energy, ΔE kcal/mol	Tafel Slope $b = \frac{RT}{\overleftarrow{\alpha}F} \times 2.303$ mV/decade	Transfer Coefficient $\overleftarrow{\alpha}$	Exchange Current Densities i_o $(A/cm^2) \times 10^6$	Activation Energy, ΔE kcal/mol
Cellulose Phenolic Resin Composite	189	903	0.10	5.5	36.5	--	--	2.66	53.8
	182	898	0.10	3.6		368	0.25	0.21	
	176	636	0.14	1.9		299	0.30	0.09	
100% Colloid 8440	178	391	0.23	3.5×10^{-1}	40	345	0.36	2.9×10^{-1}	40
	161	407	0.21	3.6×10^{-1}		276	0.31	5.1×110^{-2}	
	151	253	0.33	2×10^{-2}		237	0.26	1.3×10^{-2}	

Electrolyte: 100% H_3PO_4

Sample: Carbonized

Exposed Area: 3.74 cm^2 (geom.)

electrochemical corrosion reaction kinetics of several resin-graphite composites were studied*. To investigate the possibility that the reaction pathway may shift as the reaction advances, polarization studies were performed on 32% Varcum 29-703 composite at three different stages of the corrosion reaction. Corresponding corrosion currents observed at different polarization potentials at 182°C are reported in Figure II.5. Tafel slopes observed after 64 and 128 hours of corrosion are the same and significantly different from the slopes observed after 8 hours of corrosion. Transfer coefficients, $\vec{\alpha}$, and activation energies calculated from exchange current density vs $\frac{1}{T}$ plot (a typical plot is shown in Figure II.6) are reported in Table II.2 for each of the three different cases. Activation energies are similar for the samples corroded for 64 hours and 128 hours but significantly higher than the sample corroded for 8 hours. These kinetic parameters suggest the presence of a faster reaction during the initial period and are possibly related to the sample 'skin' corrosion. In future studies, the time dependent corrosion kinetics of other types of composites will be studied in order to understand the pronounced change in reaction kinetics noticed after the initial period and also to comprehend the corrosion reaction of bipolar plates as a whole.

D. Corrosion Rate Controlling Mechanism

All electrochemical results reported thus far in this report and in a previous report* showed that transfer coefficients and exchange current densities were distinct in two different potential ranges which, in fact, represent two dissimilar reaction mechanisms in the potential range of 0.5 to 1.0V (RHE).

The observed current density, i, at any potential, V, is represented as the sum of currents, i_1 and i_2, contributed by the individual reactions:

---

* DEN3-67, No. 5, Oct. - Dec. 1979

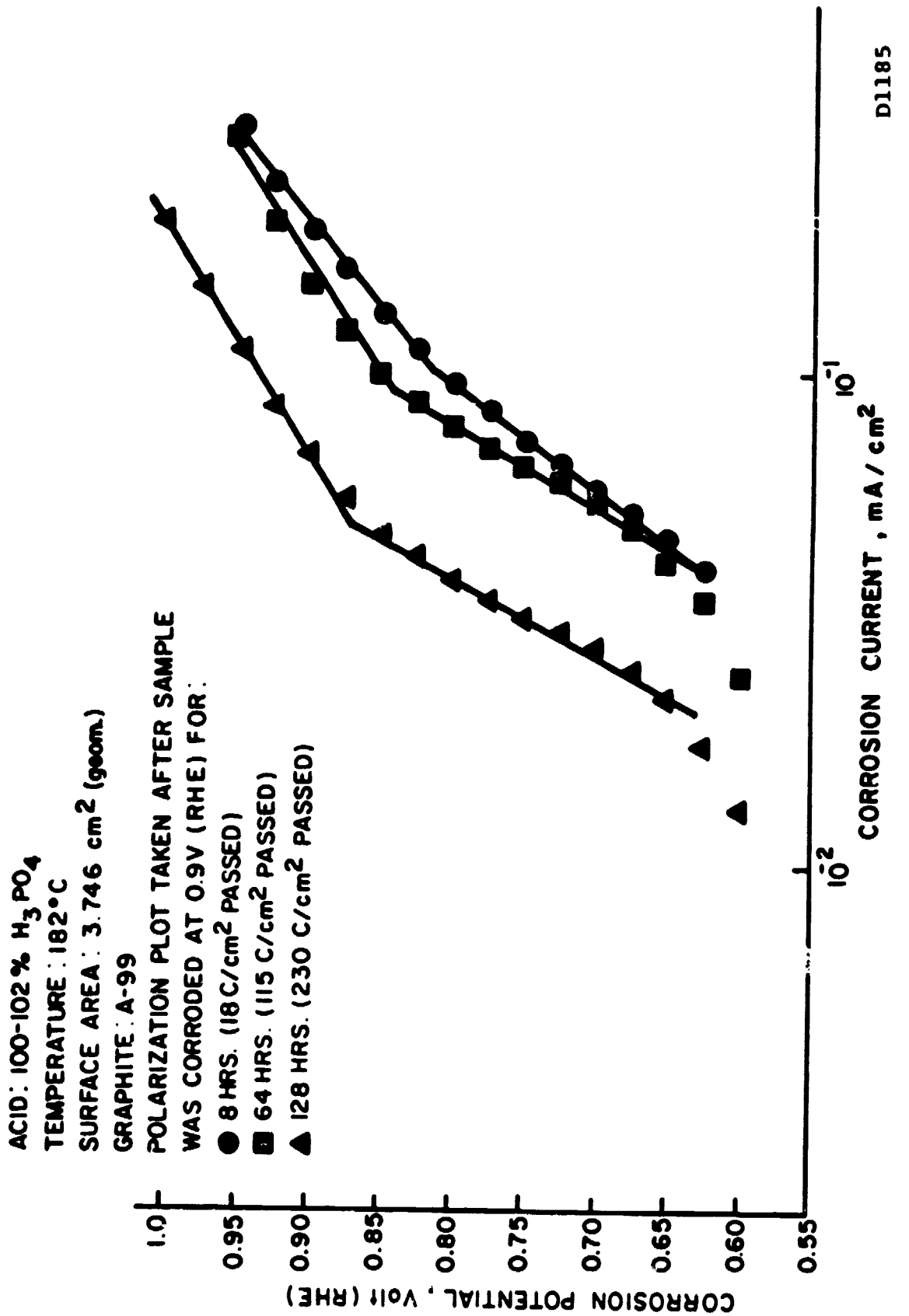

FIGURE II.5 EFFECT OF CORROSION ON THE POLARIZATION PLOT OF A 32% VARCUM 29-703 COMPOSITE

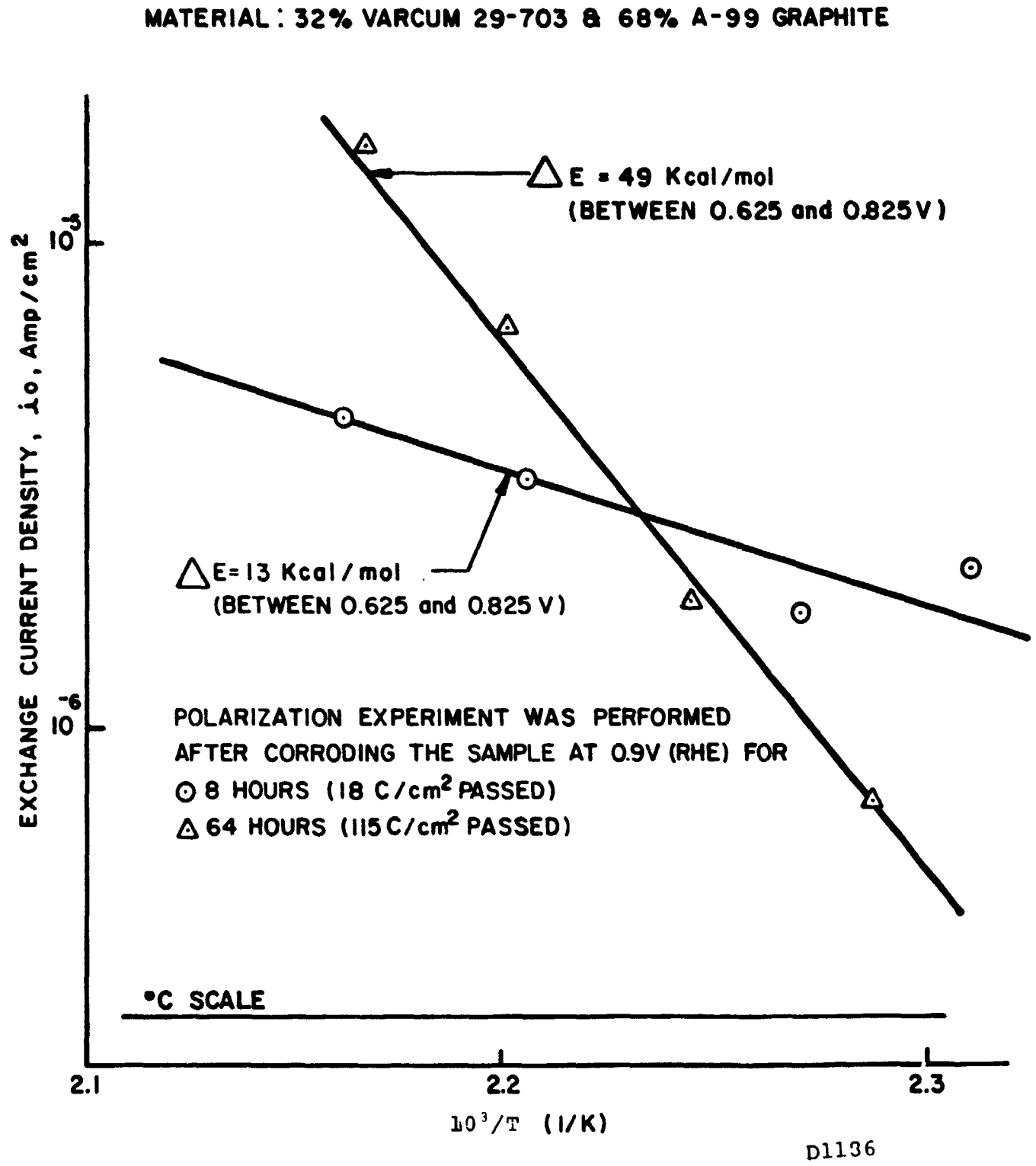

FIGURE II.6 ENERGY OF ACTIVATION

TABLE II.2

CHANGE OF REACTION PARAMETERS WITH CORROSION

CORROSION AT 0.9V(RHE) PRIOR TO POLARIZATION STUDY	0.625 to 0.825V (RHE)		0.825 to 1.0V (RHE)	
	Average Transfer Coeff. $\overleftarrow{\alpha}_1$	Activation Energy kcal/mole	Average Transfer Coeff. $\overleftarrow{\alpha}_2$	Activation Energy kcal/mole
8 hours (18 C/cm^2 passed)*	0.20	13	0.35	12
64 hours (115 C/cm^2 passed)	0.16	49	0.45	44
128 hours (230 C/cm^2 passed)	0.17	41	0.47	39

* C = coulombs

$$i = i_1 + i_2$$

$$= i_{o,1} e^{\frac{V-E_1}{RT}\overleftarrow{\alpha}_{1F}} + i_{o,2} e^{\frac{V-E_2}{RT}\overleftarrow{\alpha}_{2F}} \quad (1)$$

Where,

i_o = exchange current density

E = theoretical open circuit potential

$\overleftarrow{\alpha}$ = transfer coefficient of the anodic reaction.

The predominance of one reaction over the other depends on the electrode potential, exchange current densities, transfer coefficients and the operating temperature. Depending on the resin type, pretreatments and temperatures, the 'changeover' potential (at which the predominance of one mechanism over the other occurs) varied between 0.775 and 0.95V (RHE).

This changeover potential, evaluated from the point of intersection of two straight lines on the polarization plot for 32% Varcum 29-703 (Figure II.5), is plotted against operating temperatures for three different pretreatments (Figure II.7). The changeover potential is observed to decrease as the temperature increases because the Tafel slope of the second reaction is smaller than that of the first reaction.

Corrosion current, i_2, contributed by the second reaction increases much faster with the increase of potential (because the Tafel slope is smaller). Therefore in fuel cells, the operating potential must be maintained below the changeover potential in order to achieve longer life for cathode plates.

2.2 PHYSICAL PROPERTY MEASUREMENTS

2.2.1 Electrical Contact Resistivity

A method was developed to determine the contact resistivity between two or more contacting surfaces. The effects of area, pressure, and current on electrical contact losses were formulated in an equation. An estimation of the electrical contact losses

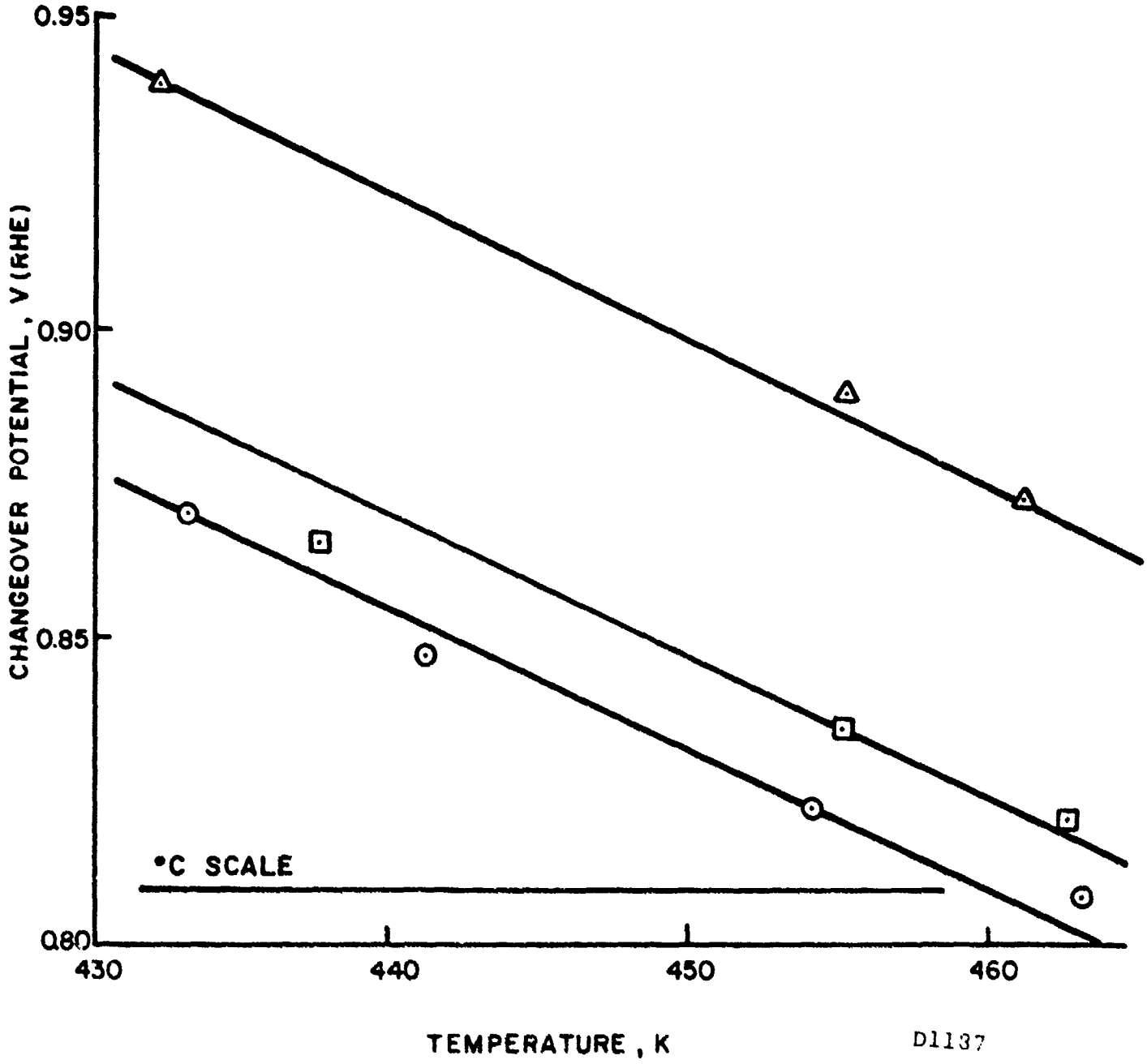

FIGURE II.7

EFFECT OF TEMPERATURE ON THE CHANGEOVER POTENTIAL OF 32% VARCUM 29-703

between phenolic/graphite composites and wetproofed backings was calculated for fuel cell stacks.

The initial experiments were conducted for two types of phenolic resin/graphite composites: 33 wt% Colloid 8440/ 67 wt% A-99 and 850 graphite; and 32 wt% Varcum 24-655/ 68 wt% A-99 graphite. For each phenolic resin/graphite material, two 5.7 cm diameter, 1.9 cm thick disks were compression molded and machined round. The disks shall be referred to as "conductors" and the material placed between the disks as "inserts", e.g., wetproofed backing paper was a type of insert (Figure II.8). The initial measurements conducted on the two 33 wt% Colloid 8440 disks were designed to determine the significance of pressure and current, and to refine the technique (Table II.3).

Figure II.8 explains the principle used to measure the voltage drop, E_4, across the contacts, using the voltage drop measurements across probes ae. E_4 is defined as:

$$E_4 = Y_4 - Y_3 \tag{2}$$

Where,

$$Y_4 = m_2X_2 + b_2 \tag{3}$$

$$Y_3 = m_1X_1 + b_1 \tag{4}$$

For conductors of the same composition,

$$m_1 = m_2 = \frac{\Delta Y}{\Delta X} = \rho_1 \frac{I}{A} \tag{5}$$

Where,

I = current,

A = Area (Cross-sectional),

$\rho_1 = \frac{VA}{I\ell}$ = resistivity of the conductors and

ℓ = path length

Substituting Equations 3, 4 and 5 into Equation 2,

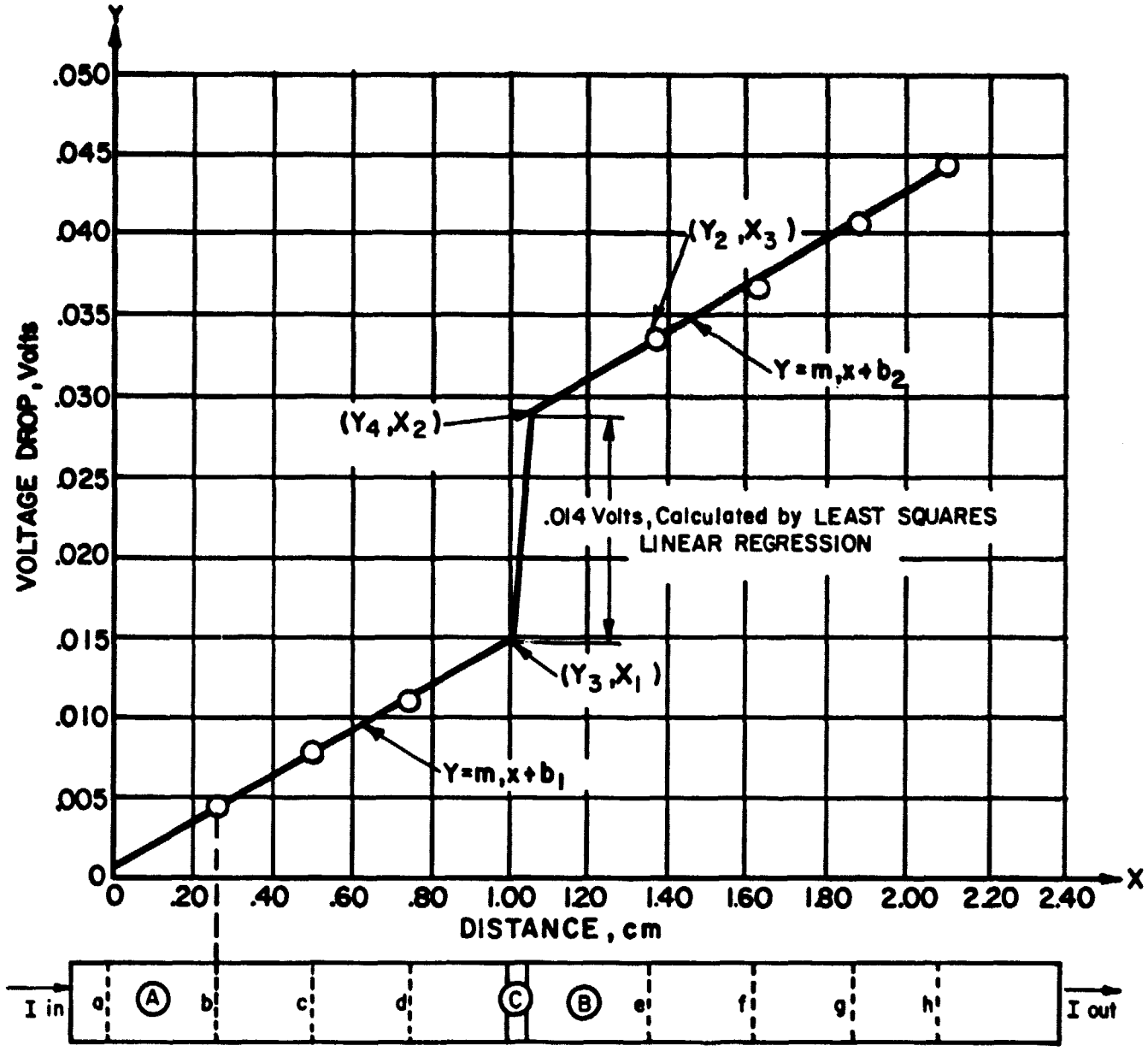

Ⓐ AND Ⓑ – 33 W% COLLOID 8440/67 W% GRAPHITE WITH A-99 AND 850 CONDUCTORS
Ⓒ BACKING, 37.4 % FEP (INSERT)

a, b, c, d, e, f, g, h ARE PROBES MEASURING VOLTAGE DROP ACROSS SAMPLES.

PARAMETERS : 1. PRESSURE – 276 kPa
2. SAMPLE CROSS SECTIONAL AREA = 11.40 cm^2
3. COLLOID 8440/GRAPHITE MATERIAL SANDED WITH 320 GRIT AL_2O_3
4. CURRENT DENSITY = 100 mA/cm^2
5. MACHINED ROUND SAMPLES

D1085A

FIGURE II.8 MEASUREMENT OF CONTACT LOSSES

TABLE II.3

CONTACT RESISTIVITY FOR 33wt% COLLOID 8440/67wt% A-99 + 850 GRAPHITE CONDUCTORS

DESCRIPTION OF EXPERIMENT	EXPERIMENT NO.	PRESSURE P, kPa	AREA A, cm^2	CURRENT I, Amps	VOLTAGE DROP, V	CONTACT RESISTANCE ohm	CONTACT RESISTIVITY, ohm $-cm^2$
Graphite composite, graphite composite contacts	5-2	276	19.25	2.00	.0108	.0054	.104
	8	"	11.39	1.174	.0160	.0140	.155
	15A1	"	0.153	.0153	.0133	.8720	.133
	15A2	552	0.153	.0153	.0059	.3830	.059
Graphite composite, FEP backing paper #10,006 (37.4w/o FEP), graphite composite contacts	6-2	276	19.25	2.00	.0142	.0071	.137
	9-1	"	11.39	1.174	.0143	.0122	.139
	15C2	552	0.153	.0153	.0044	.2900	.044
Graphite composite backing paper with no FEP, graphite composite contacts	15B1	276	0.153	.0153	.0030	.194	.030
	15B2	552	0.153	.0153	.0020	.1301	.020
Graphite composite, copper insert, graphite contacts	13-7	276	4.077	.407	1.4000	3.4410	14.0
	14-3	552	4.077	.407	.0378	0.0929	.378
Graphite composite, gold plated copper insert, graphite composite contacts	13-6	276	4.077	.407	.7890	1.9400	7.9
	14-4	552	4.077	.407	.0076	.0187	.076

Note: Conductor surfaces machined flat and sanded with 320 grit Al_2O_3

Contact Resistivity, $P\ell$: $P\ell = RA = \frac{V}{I} A$ where R = contact resistance, A = area

1kPa = ___psi

$$E_4 = \frac{\rho_1 I}{A}(X_2 - X_1) + b_2 - b_1 \qquad (6)$$

From Figure II.8

$$b_1 = 0 \qquad (7)$$

$$b_2 = Y_2 - m_1 X_3 \qquad (8)$$

(Y_2 and X_3 are experimental values).

Therefore,

$$E_4 = \frac{\rho_1 I}{A}(X_2 - X_1 - X_3) + Y_2 \qquad (9)$$

The apparent contact resistivity, ρ_2, may be defined as:

$$\rho_2 = \frac{E_4 A}{I} = \rho_1(X_2 - X_1 - X_3) + \frac{A}{I} Y_2 \qquad (10)$$

For experiments with an insert between the conductors, ρ_2 is for two contacts and the insert. The separation of backing paper resistance from electrical contact resistance requires further work. Based on the symmetry of Equation 10, the resistivity of a single contact including half the resistance of an insert, ρ_c, equals

$$\rho_c = \frac{\rho_2}{2} = \frac{E_4 A}{2I} \qquad (11)$$

Therefore in scaling to one cell, the resistance of one backing was not taken into account or, for a 23 cell stack, for example, the contact resistance calculation would include only 23 backings instead of the actual 46 backings in the stack.

Conductor resistivity, ρ_1, used for calculating ρ_2 was evaluated from a series of initial voltage drop measurements across the conductor. Least square estimates of slopes m_1 and m_2 were converted to resistivity and averaged. Using

these algorithms, a computer program was developed for data processing and calculating the contact resistances from the experimental results. Contact resistances of 32 wt% Varcum 24-655/ 68 wt% A-99 graphite disks with: no insert, backing paper insert, wetproofed backing paper insert and gold plated copper foil insert were thus measured at different applied pressures. In each experiment, Ohm's Law, V = IR, was obeyed. A typical V vs I plot when no insert was used is shown in Figure II.9. Effect of applied pressure on the contact resistance was similar for different inserts and a typical ρ_2 vs $\frac{1}{P}$ plot is shown in Figure II.10. The experimental results always agreed with the following simple relationship:

$$\rho_2 = \frac{C_1}{P} + C_2 \qquad (12)$$

Where, C_1 and C_2 are least square estimates of parameters.

In a fuel cell stack, pressure is applied on flat (non-ribbed) end plates and the stack pressure reported on the basis of the surface area of an end plate. The pressure between the ribbed bipolar plate and backing paper depends on their contacting area, A_1, and applied force, F_1.

$$P = \frac{F}{A_1} \qquad (13)$$

An equation to compute the contact resistance, R_c, in a cell between the bipolar plate and backing, and the resistance of half a backing paper can be developed by combining Equations 11, 12 and 13.

$$R_c = \frac{\rho_c}{2A} = \left(\frac{C_1 A_1}{F} + C_2\right)\frac{1}{2A} \qquad (14)$$

The following conclusions were made concerning electrical contact resistivity measurements:

1. Electrical contact resistance of graphite materials in fuel cell stacks obeys Ohm's Law, V = IR

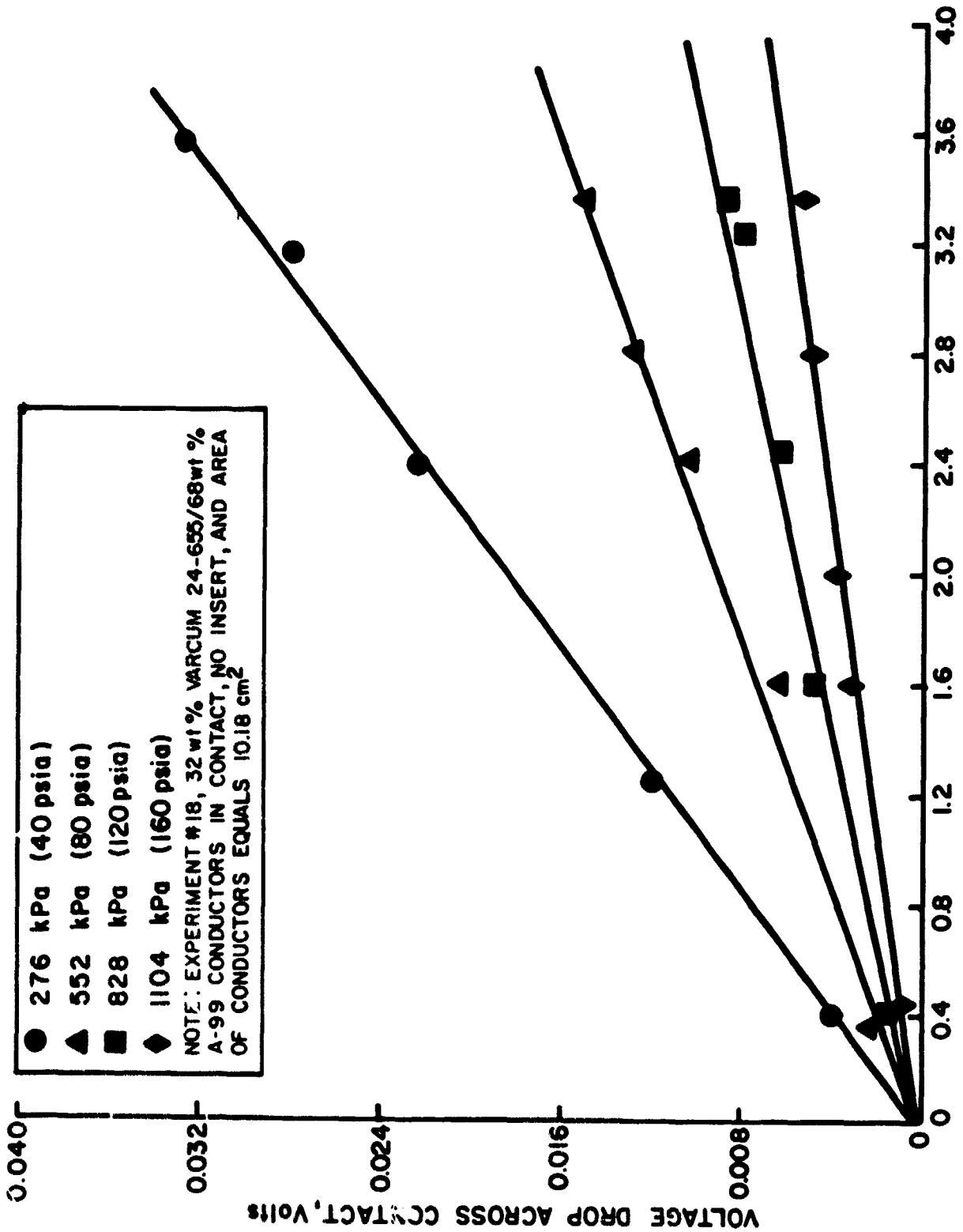

D1183

FIGURE II.9 CONTACT RESISTANCE OBEYS OHM'S LAW

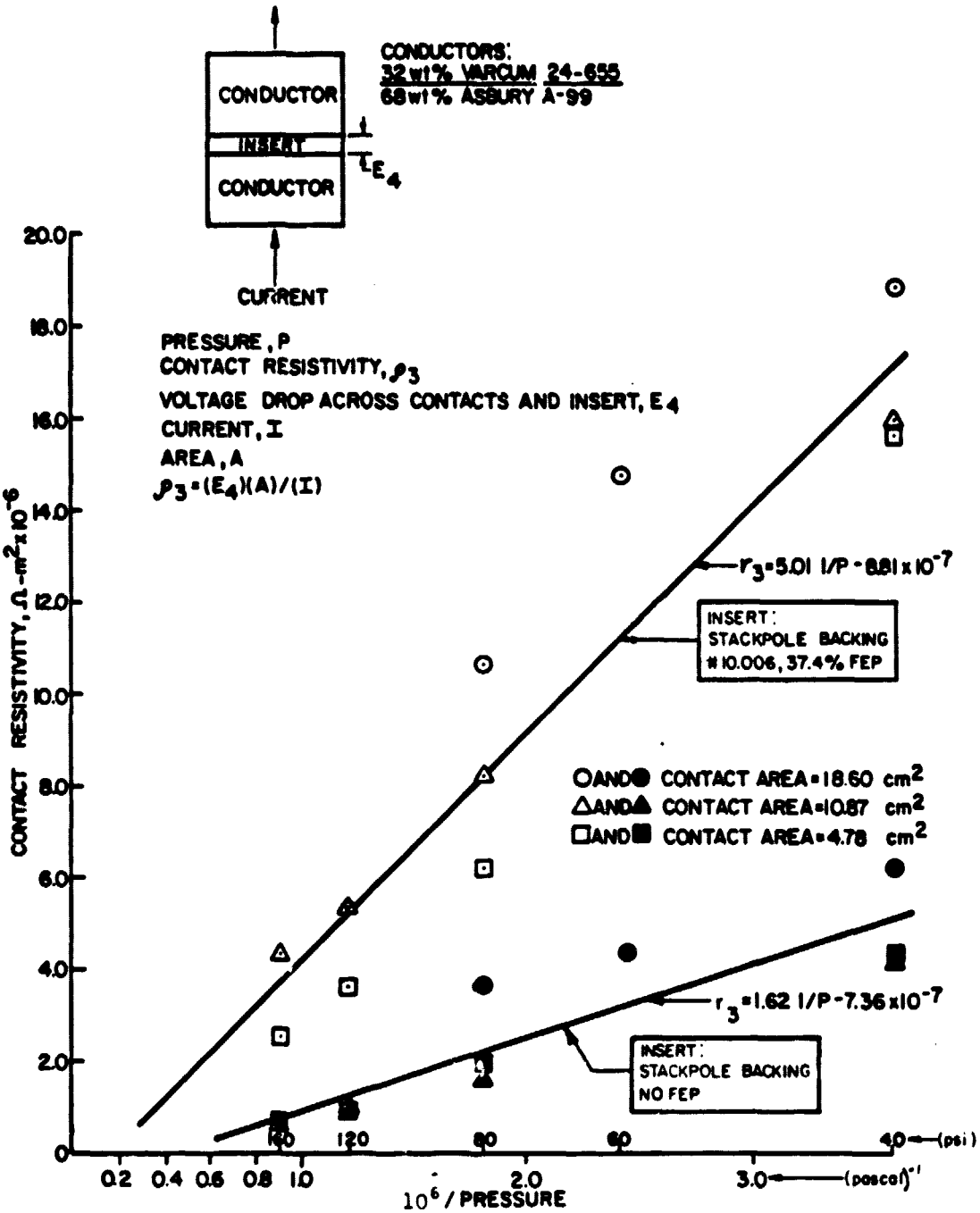

NOTE: EACH DATA POINT REPRESENTS THE AVERAGE OF 3 TO 5 VOLTAGE MEASUREMENTS AT DIFFERENT CURRENT SETTING. CONDUCTOR SURFACES SANDED WITH 320 GRIT AL_2O_3

FIGURE II.10 D1201

ELECTRICAL CONTACT RESISTIVITY WITH STACKPOLE BACKING INSERTS

2. The accuracy of the measurements was sufficient to discern differences between the various types of contacts that occur in fuel cell stacks.
3. The electrical contact resistance for current bipolar plate materials is slightly lower between plate - backing paper - plate, than between just two plates. This agrees with in-house measurement on 1200 cm^2 DIGAS coolers. The compressibility of the backing paper and irregular surface of the plates probably account for this fact.
4. The scaling of contact resistance from subscale electrical contact resistivity measurements appears feasible.
5. With constant pressure on the end plates, a reduction of contacting ribbed surface area will not affect the overall contact resistance as significantly as previously thought, because the increased pressure at the rib - backing paper interface reduces the contact resistivity.

Pertinent information on contact resistivity requiring further investigation includes:

- The accuracy and reproducibility of the measurements requires further experimentation.
- The effects of changes in area on the contact resistivity measurements needs further evaluation. Equation 5 assumes that the contact resistivity is independent of area but, as shown in Figure II.10, consistent variations were observed in contact resistivity values for the different areas. Factors which may account for these variations include: errors in length and area measurements, variability of the electrical resistivity of the conductors, and improper alignment of the conductors and insert.
- The effects of the surface condition of the conductors, changes in resin content of the conductors, and temperature on contact resistivity requires investigation.
- As previously noted, the resistance of the backing paper was not separated from contact resistivity. Measurements of backing paper resistivity will solve this problem.

In conclusion, the method for measuring contact resistivity will improve with use and will supply valuable information for fuel cells.

2.2.2 Stack Resistance

Table II.4 shows the calculated values for stack resistance. These values are present estimates and their accuracy will improve

TABLE II.4

ELECTRICAL RESISTANCE OF 12 in. x 17 in. SIZE FUEL CELL STACKS

LOCATION IN STACK	RESISTANCE, mΩ for 5-cell stack	RESISTANCE, mΩ for 23-cell stack	COMMENTS
plate resistance	0.57	2.69	Values based on dimensions of C2C2 bipolar plates, molded DIGAS coolers, and an electrical resistivity of 150 mΩ-cm.
contact resistance plate-backing interface	0.47	2.54	Values based on 37.4% FEP in backing paper, 414 kPa(60 psia) on end plates, and molded DIGAS coolers (see Figure II.10).
in-plane backing paper resistance	0.08	0.35	Values based on 37.4% FEP backing paper #10,006. In-house resistivity measurement was 19 mΩ-cm.
matrix resistance	0.22	1.02	Parameter included: 0.015 cm thick matrix with 50% porosity; 180°C H_3PO_4; and acid resistivity of 1.7 Ω-cm*.
Total:	1.34	6.60	
Actual measurement on stacks, including current collectors	4.0	12.5	
Stack resistance accounted for:	34%	53%	

* Electrical resistivity value was extrapolated from data in MacDonald, D. and Boyack, J., "Density, Electrical Conductivity and Vapor Pressure of Concentrated Phosphoric Acid," Journ. of Chem. and Eng. Data, 14, No. 3, July 1969.

as techniques are perfected. Factors accounting for the difference between the total of the calculated values and stack measurements include: the current collectors in the stack, the pressure distribution, the percent porosity of the matrix, the acid distribution, the actual electrical conductivity of the acid, and errors in physical dimension measurements for samples used in resistivity measurements.

The values in Table II.4 were determined by the following:

1. Resistance of bipolar and DIGAS plates*:
2. Contact resistance of plate - backing paper interface: See preceding Section II.2.1.
3. The in-plane resistance of backing paper was determined from in-house electrical resistivity measurements on a backing paper (#10,006, 37.4% FEP) and from physical dimensions. The in-plane resistance of a backing,

$$R_b = \frac{2\ \rho_3 \ell_3}{N_1\ t_1\ X} \qquad (15)$$

Where,

ρ_3 = the in-plane resistivity of the backing paper,

ℓ_3 = the mean path length,

t_1 = the backing paper thickness,

x = the unit length of the anode, cathode, or DIGAS rib of a plate, and

N_1 = the number of unit areas

4. The resistance of the matrix,

$$R_m = \frac{t_3\ \rho_4}{EA} \qquad (16)$$

Where,

t_3 = the matrix thickness,

* DEN3-67, No. 3, Apr. - June 1979, pp 61-62.

ρ_4 = the electrical resistivity of the electrolyte,

E_1 = the percent porosity of the matrix, and

A = the conducting or active area of the cells.

The values in Table II.4 shall be updated as improvements in measurement occur and more data is collected.

TASK III ENDURANCE TESTING

3.1 EFFECT OF OPERATING VARIABLES ON CELL PERFORMANCE AND COMPONENT DEVELOPMENT

Performance stability testing indicates that Stacks 379 exceeded 8200 hours and Stack 380 surpassed 7700 hours of operating time at the end of the quarter. Stack 379 was assembled with sheet mold electrodes and a Kynol matrix whereas Stack 380 was assembled with rolled electrodes and a SiC matrix. A discussion of Stack 379 was presented in previous reports*. A performance up-date for Stack 379 presented in Figure III.1, establishes the long-term operating capability of sheet mold electrodes. Similar electrodes have been used in a full scale stack (No. 415) which is presented in Task IV. Endurance of Stack 380 also establishes the long-term capability of stacks with a SiC matrix.

3.2 LONG-TERM COMPONENT EVALUATION

Twelve stacks have been in operation since September 1979. There are three groups of four stacks with different matrices in each group (a. Kynol, b. SiC, c. Mat-1). The evaluation of potential difficulties for long-term operation (>10,000 hr.) will be obtained from this test. Stack performance at the end of the quarter was averaged in each group and plotted as a function of operating time, as shown in Figure III.2. Stacks with Kynol matrices exhibited further decreases in performance, which is consistent with performance characteristics for Kynol stacks as discussed in the previous reporting period.

A consistent increase in ohmic resistance of these stacks is observed (Figure III.2) resulting in performance loss. A total of $\sim$ 60 mV/cell loss was observed in Kynol stacks (on an average basis of operating stacks) over 3200 hours of operation. A major portion of the 60 mV loss (35 mV/cell ohmic loss) was due to an increase in resistance from 5.6 to 8.5 mΩ/stack. The remainder of the loss is attributed to diffusion related

---

* ERC Technical Progress Report DEN3-67, Nos. 3-5, Apr. - Dec. 1979.

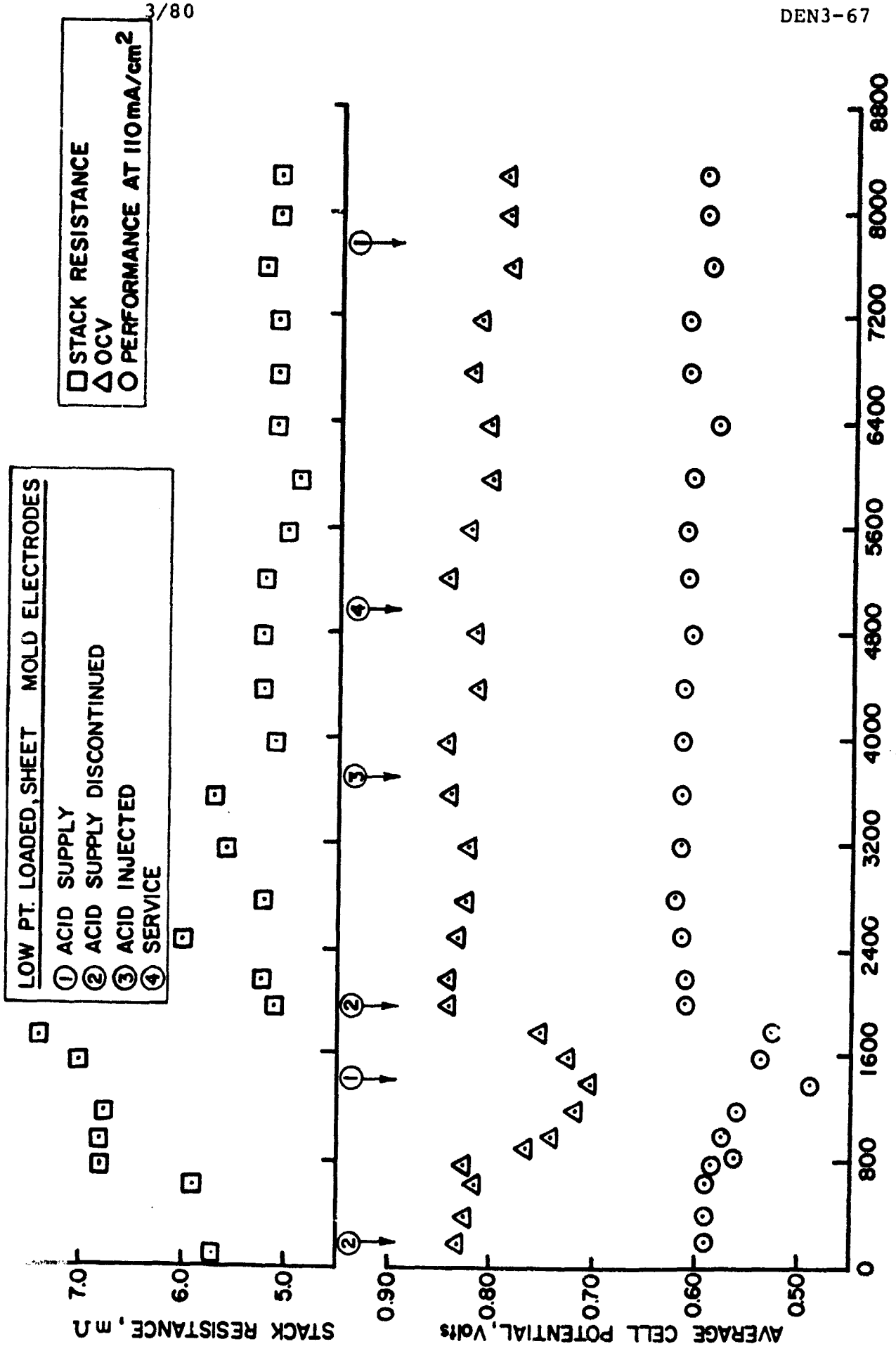

D1199

FIGURE III.1 LIFEGRAPH OF STACK 379

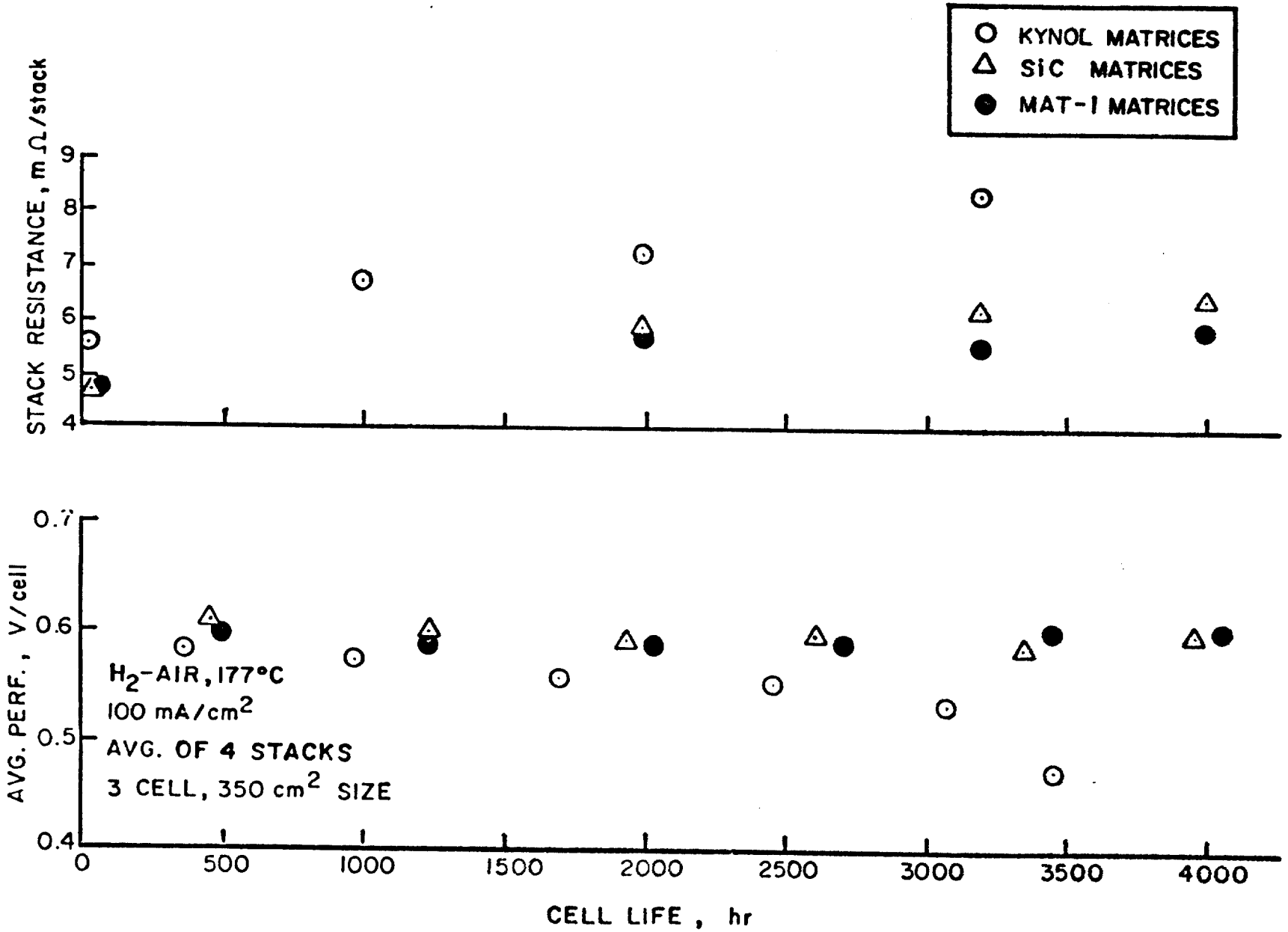

FIGURE III.2

ENDURANCE OF PAFC STACKS WITH DIFFERENT MATRICES

D1081A

and other undefined losses. Analysis of polarization curves with oxygen - hydrogen and air - hydrogen performance indicated both high Tafel slopes (100 to 150 mV/decade) and "O_2 gains" (80 to 110 mV at 100 mA/cm^2). The potential difference of cells with O_2 as oxidant to that of air at 178°C is defined as "O_2 gain". The theoretical O_2 gain for these conditions is calculated to be $\sim$ 65 mV at 100 mA/cm^2. These values appeared to be lower for the Mat-1 and SiC matrix stacks (Tafel slopes of 85 to 100 mV/decade and O_2 gain of 65 to 80 mV) than for Kynol stacks. Average ohmic resistance for these stacks is also considerably lower than for Kynol stacks (Figure III.2). The increased resistance in the Kynol matrix group may be due to structural changes in the phenolic matrix as a function of time. Most of the stacks with SiC and Mat-1 matrices appear to be stable over 4000 hours of operation (Figure III.2) and are more stable than the Kynol stacks.

TASK IV SHORT STACK TESTING

Several 1200 cm^2 short stacks (5 cell) were assembled for different purposes during this quarter. Two major changes in short stack design, as initiated during the previous quarter, are described as follows.

4.1 CURRENT COLLECTING POSITION IN THE STACK

Experimental and theoretical approaches to current collector positioning in a stack were presented previously*, including the advantages of current collection through a central post. Consequently, Stacks 412 and 413 were assembled to incorporate a central current post brazed to the copper sheet collector. Post-test analysis following testing indicated inadequate contact between the sheet and the post due to the brazing. In later stacks the design was slightly modified to ensure good contact between the current post and the sheet collector. Stacks 414 through 417 were assembled with the improved current collector design. A summary of stacks assembled during this quarter for testing is presented in Table IV.1. Test results indicated lower resistance across the terminals and gas seals after incorporating the improved current collector design.

4.2 COMPONENT AND DESIGN DEVELOPMENT

Considerable progress was realized in component and design development in full scale stacks during this quarter. The bipolar plate design was changed to incorporate a wicking channel, as described in the previous quarter. All stacks assembled after No. 414 are assembled with this improved design plate. Stacks utilizing these plates have already logged over 1100 hours of continuous operation. Lifegraphs of Stacks 415 and 416 at 100 mA/cm^2 are presented in Figure IV.1. Stack 415 was assembled with sheet mold electrodes and Kynol matrices whereas Stack 416 was assembled with rolled electrodes and Kynol matrices. Both stacks were assembled with prefilled components and began operation after a few days. The performance of both stacks was almost identical initially but then Stack 416 started to decrease slightly(Figure IV.1). No major difference in open circuit

* ERC Technical Progress Report DEN3-67, No. 5, Oct. - Dec. 1979.

TABLE IV.1 SUMMARY OF 1200 cm^2, 5-CELL STACK TESTING

STACK NO.	COMPONENT DESCRIPTION	INITIAL AVG. PERFORMANCE, volts/cell @100 mA/cm^2	LIFE, hrs.	AVG. LIFE PERF. volts/cell @ 100 mA/cm^2	REMARKS
414	Kynol matrix Rolled electrodes	0.53	768	0.51	Disassembled.
415	Kynol matrix sheet mold electrodes	0.58	1098	0.57	Prefilled components Testing in progress.
416	Kynol matrix Rolled electrodes	0.58	1100	0.56	Prefilled components Testing in progress.
417	Kynol matrix Rolled electrodes	0.56	859	0.52	Testing in progress for low FEP on anode.
419	Mat-1 matrix Rolled electrodes	--	--	--	Wicking test indicated prolonged period of wicking time.
423	Mat-1 matrix Rolled electrodes	0.59	30	0.59	Wet assembled.

Note: Stacks 421 and 422 are being wicked. These stacks are dry assembled with Mat-1 matrices.

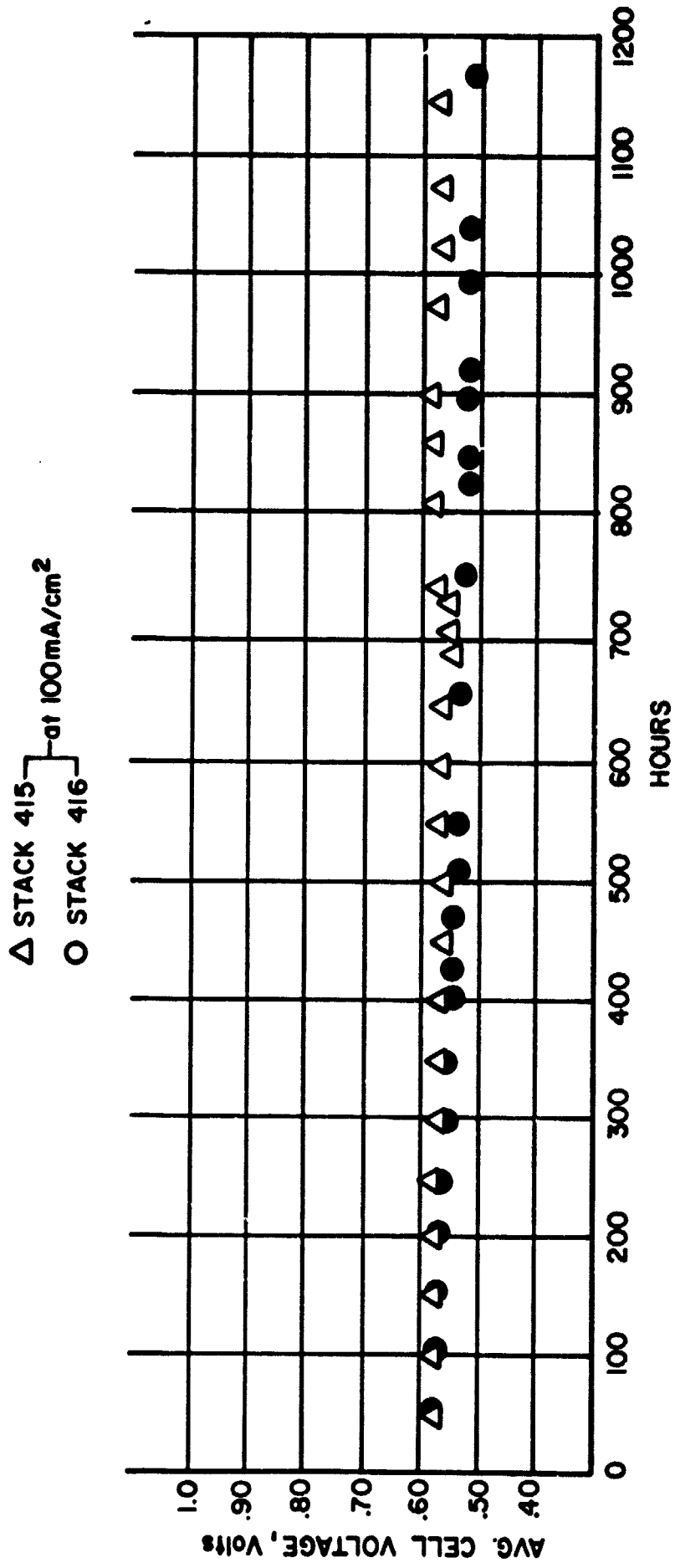

D1189

FIGURE IV.1

LIFEGRAPHS OF STACKS 415 AND 416

voltage and stack resistance was observed (not shown in the figure). Analysis of polarization data at 1000 hours of operation for both stacks indicated higher Tafel slopes and O_2 gains in the stack with rolled electrodes (Stack 416) than for the one with sheet mold electrodes (Stack 415). This may be the reason for the performance variations in the stacks.

Stack 415 also demonstrated the long-term operating capability of sheet mold electrodes in full scale stacks. The performance data for a medium size (350 cm^2) stack is presented in Section 3.2. A combination of sheet mold electrodes and Mat-1 matrices is being assembled in a 1200 cm^2, 5-cell stack for testing.

Stacks 418, 419, 421 and 422 were dry assembled with rolled electrodes and Mat-1 matrices. The usual method of wicking these stacks takes more than 4 weeks. Stacks with Kynol matrices require only about 10 to 12 days of wicking time. In order to evaluate the wickability of Mat-1 stacks, a 2 cell stack was disassembled after 3 weeks of wicking. When disassembled the top portion of the cells was found very dry. While improvements in the wicking rate for Mat-1 matrices continued, Stack 423 was assembled with prefilled, rolled electrodes and Mat-1 matrix. The stack started to operate on the following day, and by the end of the quarter, it had accumulated 30 hours of continuous operation with an average performance of 0.59 V/cell. Additional stacks are planned next quarter for testing the wet assembled stacks with Mat-1 matrices.

TASK V LONG STACK TESTING

5.1 2 kW STACK TESTING

The second 2 kW stack, No. 410, which operated for 40 hours of net running time (from Run No.1 through 7) showed overheating (~197°C) during Run No.7 due to crossleakage in the cell.

When rewicked and tested for OCV and load performances, it regained OCV without any crossleakage, but performance dropped due to increased stack resistance (14 mΩ from a previous 12 mΩ) and flooding. Table V.1 summarizes the results for the 3 day on/off running condition (Runs 8, 9 and 10): approximately 500 mV at 100 mA/cm^2 was decayed from the previous stack run. From a 2 mΩ increase in resistance, a 226 mV decay was expected. However a greater decay has been encountered, probably due to increased flooding of cell components.

Temperature profiles were again measured during Run 8. No significant change was observed in the temperature profile as compared with that obtained during Run No. 5*.

For the next 2 kW stack, acid channels will be incorporated in the bipolar plates to allow acid addition while the stack is running. A Mat-1 matrix will also be used to retain more acid in the cell. Through the new stack acid replenishing technique, the following will be evaluated for final long-term endurance testing: performance characteristics for the new matrix cells; and various physical characteristics such as acid duration, wicking rate, stack IR, flow and temperature distributions, and sealing.

*ERC Technical Progress Report DEN3-67, No. 5, Oct. - Dec. 1979.

TABLE V.1 SUMMARY OF 2kW STACK (No. 410)

(Daily on/off running)

CELL NO.	OCV, volt			PERFORMANCE @ 100 mA/cm^2, volt		
	Run No. 8*	Run No. 9†	Run No. 10†	Run No. 8	Run No. 9	Run No. 10
1	0.94	0.86	0.86		0.43	0.45
2	0.91	0.87	0.85		0.53	0.54
3	0.93	0.86	0.82		0.56	0.58
4	0.91	0.87	0.83		0.55	0.55
5	0.83	0.83	0.82		0.50	0.50
6	0.91	0.86	0.83		0.56	0.56
7	0.91	0.85	0.82	No Test	0.55	0.56
8	0.91	0.85	0.84	at 100 mA/cm^2	0.57	0.57
9	0.92	0.86	0.83		0.55	0.54
10	0.87	0.84	0.83		0.53	0.53
11	0.89	0.83	0.81		0.56	0.55
12	0.87	0.84	0.84		0.54	0.54
13	0.85	0.83	0.72		0.53	0.53
14	0.93	0.87	0.93		0.59	0.59
15	0.88	0.84	0.82		0.51	0.50
16	0.87	0.82	0.80		0.56	0.56
17	0.89	0.82	0.81		0.58	0.58
18	0.88	0.82	0.78		0.54	0.54
19	0.89	0.84	0.80		0.53	0.54
20	0.87	0.71	0.66		0.49	0.47
21	0.75	0.83	0.89		0.54	0.50
22	0.98	0.84	0.80		0.52	0.54
23	0.88	0.85	0.79		0.39	0.44
Total	20.47	19.29	18.78		12.21	12.26

*OCV at 120°C
†OCV at 175°C

5.2 2 kW STACK TEST STAND IMPROVEMENTS

Design of additional safety features was initiated to prevent cell damage during unattended operation. As shown in Figure V.1, when any one of the failures (stack overheating, short-circuit, current load and air fan failures) occurs, the stack is automatically shut down by subsequent shut-off of fuel and air flows, releasing current load, and turning off heaters. Then the stack is kept at a lower temperature by auxiliary heaters (which prevents moisture absorption).

5.3 REFORMER TESTING

Methane reforming at five different space velocities ranging from 565 to 1135 hr^{-1} was performed and showed the feasibility of meeting the hydrogen supply for a 2 kW fuel cell stack. At present, a space velocity of 1200 hr^{-1} (required for 2 kW power) was examined to show that the reformer had sufficient heating capacity to obtain 100% fuel conversion. Figure V.2 shows the temperature profiles experienced in the present reformer at a space velocity of 1200 hr^{-1}. Table V.2 shows the reforming product compositions for the experimental and theoretical calculations. The conversions of 81 vs 84% for experiment vs theory at a reforming temperature of 592°C, shown in the table, indicate that the present reformer is close to equilibrium operation. Once the reforming temperature is increased, the present reformer seems capable of producing enough hydrogen for the 2 kW stack.

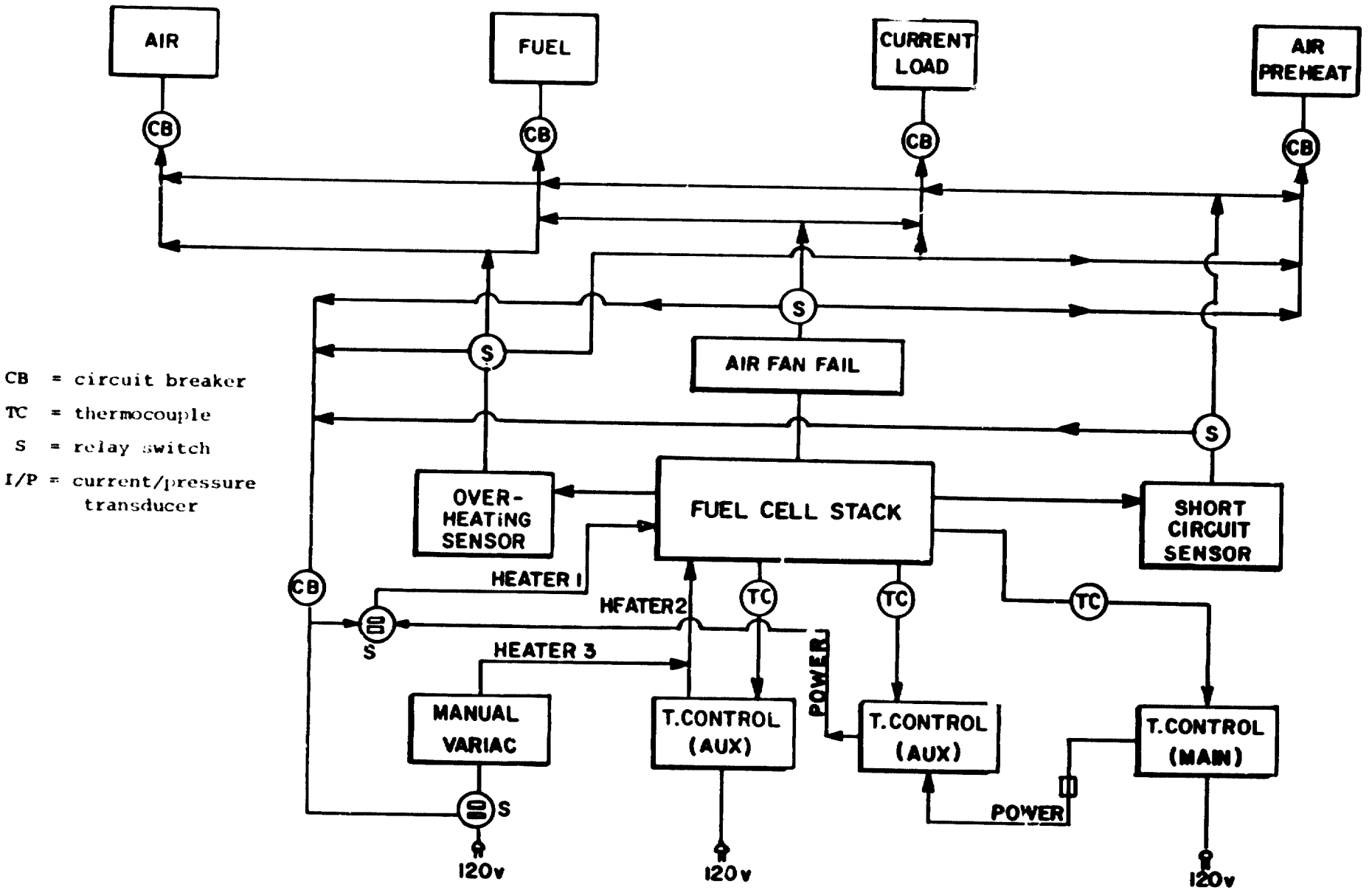

FIGURE V.1 SCHEMATIC DIAGRAM OF SAFETY FEATURES FOR 2kW TEST STAND

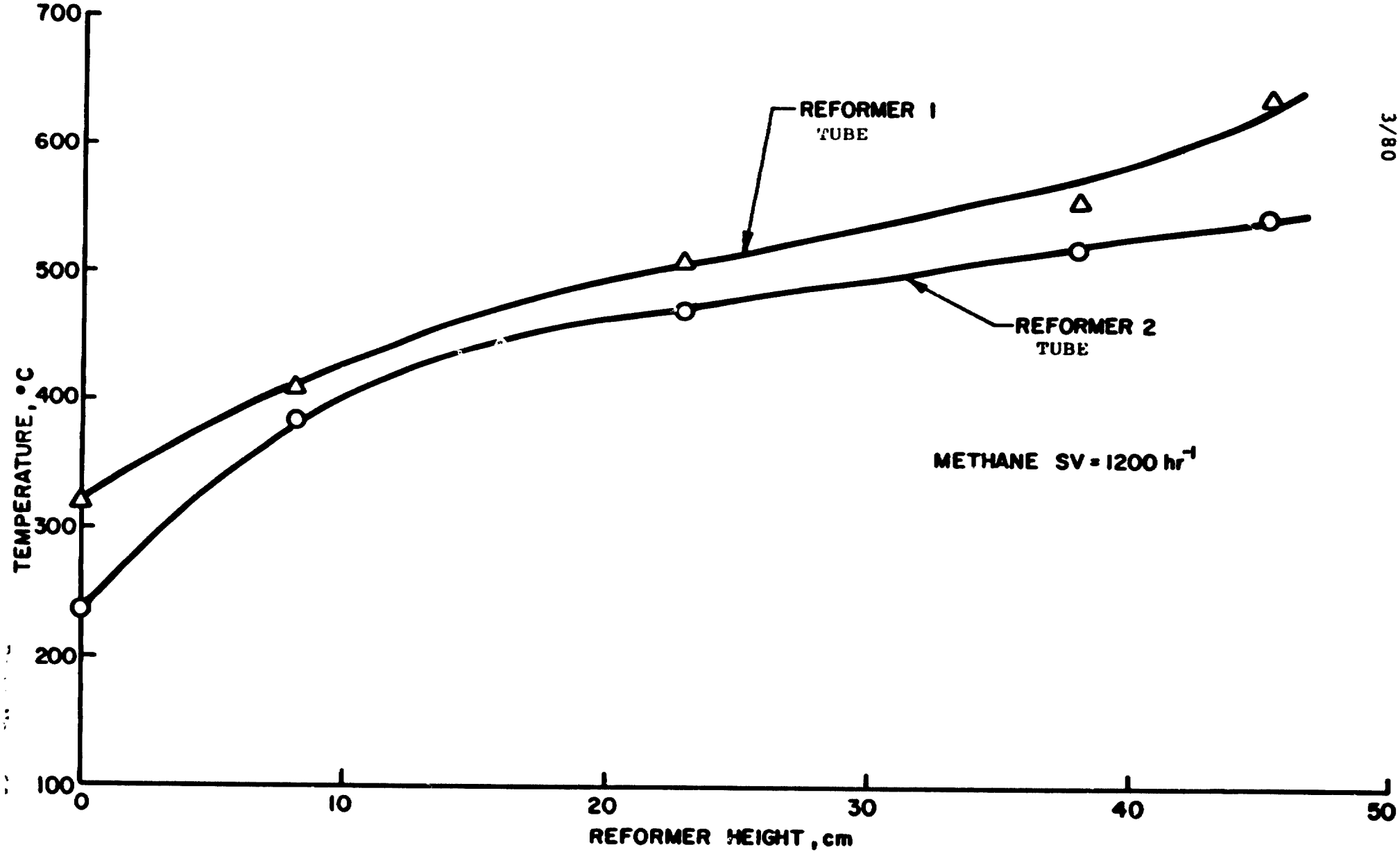

FIGURE V.2

TEMPERATURE PROFILES IN THE REFORMERS

D1190

3/80

DEN3-67

TABLE V.2

COMPARISON OF EXPERIMENTAL AND THEORETICAL METHANE REFORMING PRODUCT COMPOSITIONS

COMPOSITION	EXPERIMENTAL, %	THEORETICAL, %	COMMENTS
CH_4	2.7	2.2	• Steam/carbon = 4.37
CO	3.6	3.5	• Hydrogen/carbon = 0.1
CO_2	7.7	8.3	• Reformer Inlet Temp. = 280°C
H_2	43.5	45.0	
H_2O	42.5	40.0	• Reformer Exit Temp. = 592°C
Conversion	80.6	84.3	

APPENDIX A

ESTIMATION OF WATER VAPOR PRESSURE IN THE CELL

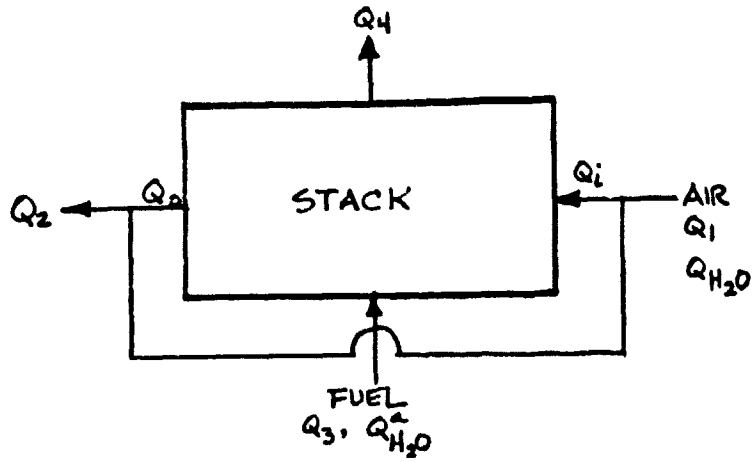

Overall mass balance:

$$Q_i - Q_o = (J_{H_2O} - 1/2\ r_{H_2O}) \cdot A$$

$$Q_3 - Q_4 = (r_{H_2O} - J_{H_2O}) \cdot A$$

Where J_{H_2O} is water flux from cathode to anode.

r_{H_2O} is water generation on cathode $\left(= \frac{I}{mF} \right)$

A is cell area.

Using arithmetic average,

$$Q^c_{avg} = RF\ (Q_i + Q_o)/2 = RF \cdot (2Q_i - J_{H_2O} \cdot A + 1/2 \cdot r_{H_2O} \cdot A)/2$$

$$Q^a_{avg} = (Q_3 + Q_4)/2 = (2 \cdot Q_3 - r_{H_2O} \cdot A + J_{H_2O}\ A)/2$$

Where RF = Fraction of air flow through cathode channels

For H_2O, the total moisture flow-in will be

$$(Q_{H_2O})_{in} = RL \cdot (Q_{H_2O})_{out} + Q_{H_2O}$$

Where RL = Fraction of air recycle

$$\therefore (Q^c_{H_2O})_{in} = RF \cdot (Q_{H_2O})_{in}$$

$$(Q^c_{H_2O})_{out} = (Q^c_{H_2O})_{in} + (r_{H_2O} - J_{H_2O})A$$

$$(Q_{H_2O})_{out} = (Q_{H_2O})_{in} + (r_{H_2O} - J_{H_2O})A$$

$$= RL \cdot (Q_{H_2O})_{out} + (r_{H_2O} - J_{H_2O})\, A + Q_{H_2O}$$

$$\therefore (Q_{H_2O})_{out} = \frac{1}{1-RL}\left[(r_{H_2O} - J_{H_2O})A + Q_{H_2O}\right]$$

$$\therefore (Q^c_{H_2O})_{out} = \left(\frac{RF \cdot RL}{1-RL} + 1\right)\left(r_{H_2O} + J_{H_2O}\right) A + \frac{RF}{1-RL}\, Q_{H_2O}$$

$$\therefore (Q^c_{H_2O})_{in} = \frac{RF \cdot RL}{1-RL}\left(r_{H_2O} - J_{H_2O}\right) A + \frac{RF}{1-RL}\, Q_{H_2O}$$

$\therefore$ Average Mole Fraction of H_2O Vapor $= X_{H_2O}$

$$= \frac{\left\{\left(\frac{2RF \cdot RL}{1-RL} + 1\right)\left(r_{H_2O} - J_{H_2O}\right)A + \frac{RF}{1-RL}\, Q_{H_2O}\right\}}{RF \cdot \left(2Q_i - J_{H_2O}\, A + r_{H_2O}\, A/2\right)}$$

$$\therefore P^c_{H_2O} = 760\, X_{H_2O}$$

For the anode side,

$$P^a_{H_2O} = 760 \cdot \left(\frac{2 \cdot Q^a_{H_2O} + J_{H_2O} \cdot A}{2Q_3 - r_{H_2O} A + J_{H_2O} A}\right)$$

When the make-up air has a mole fraction of H_2O ($\bar{Y}_{H_2O}$)

$$Q_{H_2O} = (Q_i - RL \cdot Q_o) \cdot \bar{Y}_{H_2O}$$

$$\therefore Q_{H_2O} = \left[(1-RL)\, Q_i - RL\left(\frac{r_{H_2O}}{2} - J_{H_2O}\right) A\right] \cdot \bar{Y}_{H_2O}$$

ENERGY RESEARCH CORPORATION

APPENDIX B

CORRELATION OF WATER VAPOR PRESSURE AND DENSITY OF ACID AS A FUNCTION OF T & W

(1) For water vapor pressure,

$$\log_{10} P_{H_2O} = A + B/T \qquad (1)$$

where $A = A(1) + A(2)x + A(3)x^2 + A(4)x^3 + A(5)x^4$

$B = B(1) + B(2)x + B(3)x^2 + B(4)x^3 + B(5)x^4$

where $x = \dfrac{W}{5.440 - 0.0444 \cdot W}$

For $130 \leq T \leq 170$°C and $80 \leq W \leq 101$% (MacDonald and Boyack, p 380, J. of Chem. Eng. Data, Vol 14, 1949),

$A(1) = 1.073502 \times 10$	$B(1) = -2.83625 \times 10^3$
$A(2) = -7.40558 \times 10^{-2}$	$B(2) = 1.81247 \times 10$
$A(3) = 5.46493 \times 10^{-4}$	$B(3) = -1.25648 \times 10^{-1}$
$A(4) = 1.03388 \times 10^{-8}$	$B(4) = -8.16949 \times 10^{-4}$
$A(5) = 0.0$	$B(5) = 0.0$

For T<130°C, W<102%,

A(1) = 10.6541, and the rest of the coefficients are the same.

For T>170°C, W>102%

A(1) = 10.63811, and the rest of the coefficients are the same.

For $102 \leq W \leq 105$%,

$A(1) = 2.40058 \times 10^2$	$B(1) = -8.49288 \times 10^4$
$A(2) = -4.29532$	$B(2) = 1.52987 \times 10^3$
$A(3) = 1.27542 \times 10^{-2}$	$B(3) = -4.55644$
$A(4) = 1.44261 \times 10^{-7}$	$B(4) = -5.2044 \times 10^{-2}$
$A(5) = -7.16712 \times 10^{-7}$	$B(5) = 2.57801 \times 10^{-4}$

For W>105%,

$A(1) = 1.27857 \times 10$	$B(1) = 1.38898 \times 10^3$
$A(2) = -3.25561 \times 10^{-2}$	$B(2) = -8.56829 \times 10$
$A(3) = 6.16028 \times 10^{-5}$	$B(3) = 4.57713 \times 10^{-1}$
$A(4) = 0.0$	$B(4) = -8.2059 \times 10^{-4}$
$A(5) = 0.0$	$B(5) = 0.0$

(2) For density (MacDonald and Boyack),

$$\text{Density} = 0.68235 + 0.0120811 \cdot W - \\ -(1.2379 - 3.7938 \times 10^{-3} \times W)/1000$$